

THE H II REGION KR 140: SPONTANEOUS FORMATION OF A HIGH-MASS STAR

D. R. BALLANTYNE,¹ C. R. KERTON,² AND P. G. MARTIN

Canadian Institute for Theoretical Astrophysics, University of Toronto, Toronto, ON, Canada M5S 3H8; ballanty@cita.utoronto.ca, kerton@cita.utoronto.ca, pgmartin@cita.utoronto.ca

Received 1999 November 15; accepted 2000 March 16

ABSTRACT

We have used a multiwavelength data set from the Canadian Galactic Plane Survey (CGPS) to study the Galactic H II region KR 140, both on the scale of the nebula itself and in the context of the star-forming activity in the nearby W3/W4/W5 complex of molecular clouds and H II regions. From both radio and infrared data we have found a covering factor of about 0.5 for KR 140, and we interpret the nebula as a bowl-shaped region viewed close to face on. Extinction measurements place the region on the near side of its parent molecular cloud. The nebula is kept ionized by one O8.5 V(e) star, VES 735, which is less than a few million years old. CO data show that VES 735 has disrupted much of the original molecular cloud for which the estimated mass and density are about $5000 M_{\odot}$ and 100 cm^{-3} , respectively. KR 140 is isolated from the nearest star-forming activity, in W3. Our data suggest that KR 140 is an example of spontaneous (i.e., nontriggered) formation of, unusually, a high-mass star.

Subject headings: H II regions — infrared: ISM: continuum — ISM: individual (KR 140) — radio continuum: ISM — radio lines: ISM — stars: formation

1. INTRODUCTION

Massive OB stars are almost always found in clusters. In fact, accumulating observational evidence suggests that most stars, regardless of mass, actually form as members of some kind of group, cluster, or association. While there has been progress in understanding the processes involved in the formation of a single star (e.g., Shu, Adams, & Lizano 1987), theories of cluster formation are still in their infancy (see the recent reviews by Elmegreen et al. 2000; Clarke, Bonnell, & Hillenbrand 2000). Nevertheless, many important issues have already been identified. Foremost among these is the question of whether the formation of clusters, particularly ones with OB stars, are triggered by external agents (Elmegreen 1992) such as expanding H II regions (Elmegreen & Lada 1977) or colliding molecular clouds (Loren 1976, 1977; Scoville, Sanders, & Clemens 1986; Usami, Hanawa, & Fujimoto 1995). Despite triggered or sequential star formation being theoretically and intuitively appealing, determining unambiguously a cause-and-effect relationship is a major problem because of the long time-scales (and time lags) of the processes involved. There is observational evidence for regions that have had triggered star formation, both on large scales (e.g., IC 1396; Patel et al. 1998) and on small scales (e.g., IC 1805; Heyer et al. 1996). However, there are other young star-forming regions, like Taurus, where no evidence of a trigger can be found. These are often in modest-sized molecular clouds and contain only lower mass stars.

The Perseus Arm star-forming regions W3/W4/W5 (Westerhout 1958) have been studied extensively over the last 20 years (e.g., Lada et al. 1978; Braunsfurth 1983; Digel et al. 1996; Normandeau, Taylor, & Dewdney 1997; Heyer & Terebey 1998). They are often considered to be the archetypical examples of how the formation of massive star clusters can be triggered by the influence of other nearby clusters. For example, W3 is thought to have been trig-

gered by the expansion of W4 (Dickel 1980; Thronson, Lada, & Hewagama 1985; van der Werf & Goss 1990), and there is evidence that the expansion of W5 is also triggering star formation (Vallée, Hughes, & Viner 1979; Wilking et al. 1984).

In new high-resolution multiwavelength (radio and mid-infrared) data of the W3/W4/W5 complex from the Canadian Galactic Plane Survey (CGPS; English et al. 1998), we have identified a star-forming region containing a single O star. Figure 1 shows a 1420 MHz continuum image from the CGPS pilot project (Normandeau et al. 1997). The circled area is the H II region in question, KR 140 ($l = 133^{\circ}425$, $b = 0^{\circ}055$; Kallas & Reich 1980). This region appears to be completely separate from the vigorous star formation going on nearby in W3, although it is in the same Perseus arm molecular complex (see context in CO images in Heyer et al. 1998). What is unusual is that this massive star seems to have been formed spontaneously.

In this paper we present and analyze the multiwavelength data on KR 140 in order to quantify the properties of this region of spontaneous massive star formation. As described in § 2 these data have sufficient resolution ($1'$) to resolve this H II region for the first time and reveal a fairly symmetrical structure. Based on first impressions, we thought that KR 140 might prove to be a “textbook” spherical H II region. Instead, we find that KR 140 is likely a bowl-shaped H II region (an example of a blister geometry; Israel 1978, Yorke et al. 1989; §§ 3, 4.2.2, and 6.4). We have found that the H II region is kept ionized by an O8.5 V(e) star, VES 735, and is at a distance of 2.3 ± 0.3 kpc from the Sun (Kerton, Ballantyne, & Martin 1999).

We analyze the ionized component of KR 140 in § 4 and make various estimates of the age in § 5. The dust, molecular, and atomic components of KR 140 are examined in §§ 6, 7, and 8, respectively. In § 9 we discuss star formation in KR 140 in the context of the Perseus arm and the possible accompanying cluster.

2. THE MULTIWAVELENGTH DATA

KR 140 was initially cataloged in a 1420 MHz radio continuum survey of the northern Galactic plane with the

¹ Present address: Institute of Astronomy, Madingley Road, Cambridge, United Kingdom CB3 0HA.

² Present address: Dominion Radio Astrophysical Observatory, PO Box 248, Penticton, BC, Canada V2A 6K3.

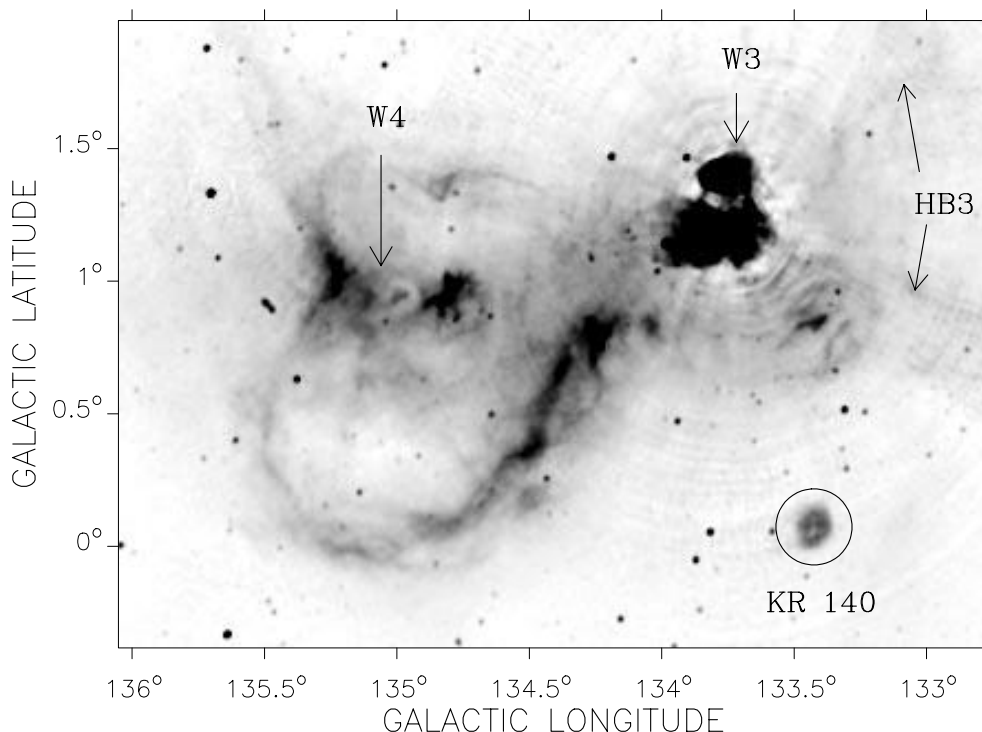


FIG. 1.—KR 140 in context. This 1420 MHz continuum image of the CGPS pilot region survey shows KR 140 (circled) in relation to the W3/4/5 star-forming regions and the HB 3 supernova remnant. The gray scale is linear with a white value of 2.0 K and a black value of 15.0 K. W5 is off the figure to the east ($l \approx 137^\circ\text{--}138^\circ$).

Effelsberg 100 m telescope by Kallas & Reich (1980). At the available resolution of $9'$ KR 140 was barely resolved, with a reported diameter of about $11'$. Although KR 140 was measured in other subsequent single-dish surveys (§ 4.2), it had never been examined with a radio interferometer to provide the angular resolution necessary for the present study.

The data analyzed here include 1420 MHz (λ 21 cm) and 408 MHz (λ 74 cm) continuum images from the Dominion Radio Astrophysical Observatory (DRAO) Synthesis Telescope (Roger et al. 1973; Veidt et al. 1985). An H I 21 cm line data cube is also available, with a spectral resolution of 2.64 km s^{-1} and a channel spacing of 1.65 km s^{-1} . These DRAO data were obtained during the pilot project of the CGPS (Normandeau et al. 1997) and made into a full $8^\circ \times 5^\circ$ mosaic of the W3/W4/W5 star-forming regions.

We also made use of a CO ($J = 1 \rightarrow 0$, 115 GHz, λ 2.60 mm, spectral resolution 0.98 km s^{-1}) data cube from the Five Colleges Radio Astronomy Observatory (FCRAO) obtained in the complementary survey described by Heyer et al. (1998). To examine the dust components we processed *Infrared Astronomical Satellite* (IRAS) data to make HIRES mosaics at 12, 25, 60, and $100 \mu\text{m}$. Independent processing of the entire Galactic plane data at 60 and $100 \mu\text{m}$ has been released as the *IRAS* Galaxy Atlas (IGA; Cao et al. 1997), and we have completed a complementary project at 12 and $25 \mu\text{m}$ (Mid-Infrared Galaxy Atlas [MIGA]; Kerton & Martin 2000).

An important feature for subsequent analysis with these data sets is the common relatively high angular resolution achieved. The DRAO synthesis telescope images have a resolution of $1' \times 1.14'$ at 1420 MHz (the 408 MHz DRAO data have proportionately 3.5 times lower resolution), and the CO images are at a resolution of $50''$ (beam sampled).

The HIRES images have noncircular beams of size about $2'$ at $100 \mu\text{m}$, $1'$ at $60 \mu\text{m}$, and somewhat less at 12 and $25 \mu\text{m}$. For detailed comparison, pairs or groups of images have been convolved to the same beam shape.

3. A MODEL FOR THE THREE-DIMENSIONAL MORPHOLOGY

Analysis of an H II region benefits from a knowledge of its three-dimensional structure, but often the observed two-dimensional morphology is too complex to interpret. Fortunately, this is not the case for KR 140. Figure 2 shows the four HIRES images of KR 140 at 12, 25, 60, and $100 \mu\text{m}$. As discussed in § 6, the $100 \mu\text{m}$ image best describes the dust distribution in KR 140. The $100 \mu\text{m}$ HIRES image (Fig. 2*d*) shows that most of the dust in the nebula has been swept into a shelllike structure and that we are observing a region that is close to being circularly (axially) symmetric. In the 1420 MHz image (Fig. 3) KR 140 is also seen to be fairly circular with a central depression. As highlighted by the contour map, there are three high-intensity areas: two “eyes” and a “mouth.” However, where the “nose” would be is a lower intensity area. The simplest interpretation appears to be a three-dimensional structure with a central hole (§ 5.2.2). We have identified VES 735 as the exciting star of this H II region (Kerton et al. 1999); it lies projected close to this lower intensity area of H II emission, though not coincident with it.

Since we have also classified the exciting star, we can draw further conclusions about the geometrical structure of KR 140 from a global analysis (§ 5 in Kerton et al. 1999). Even after taking into account the emission from dust that was not observed by *IRAS*, we find that the total luminosity of warm dust in the nebula is far less than the bolometric luminosity of the ionizing star VES 735 and that the cover-

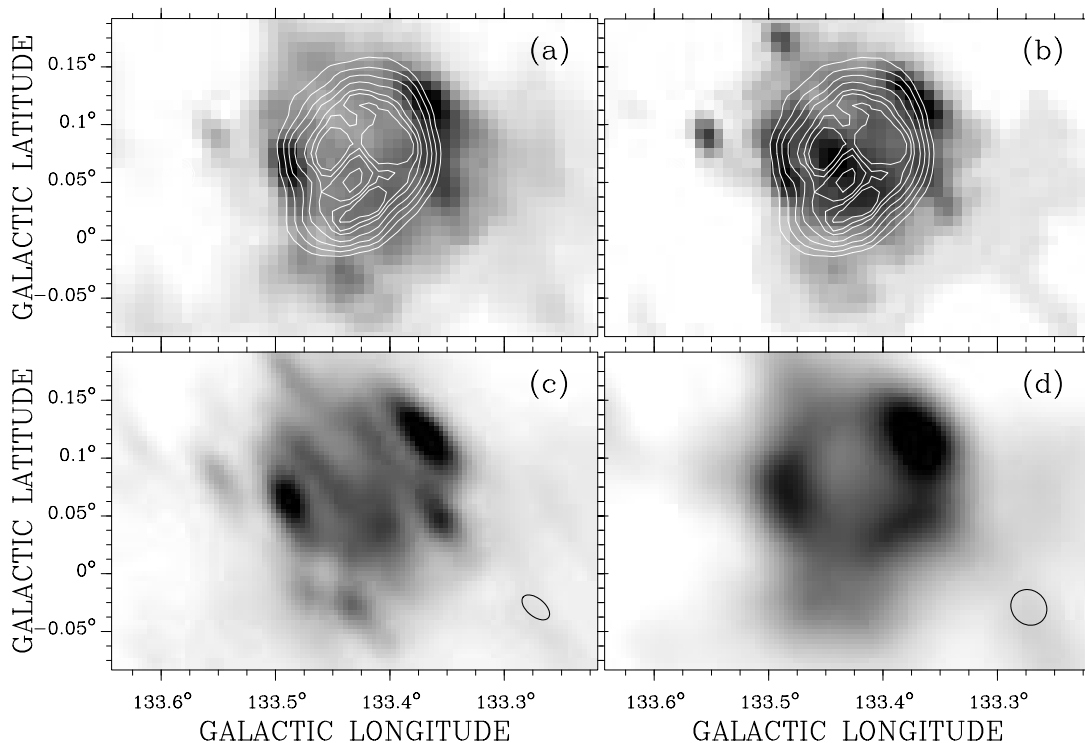


FIG. 2.—(a) 12 μm HRES image convolved to 1420 MHz resolution and then overlaid with 1420 MHz contours. The contour values are the same as Fig. 3a. The gray scale is linearly scaled from 2.0 to 20.0 MJy sr^{-1} (white to black). (b) 25 μm HRES image convolved to 1420 MHz resolution and then overlaid with 1420 MHz contours. The contour values are the same as Fig. 3a and the image is scaled from 4.0 to 25.0 MJy sr^{-1} (white to black). (c) Original 60 μm HRES image. The beam shape is shown in the lower right-hand corner. The image is scaled from 10.0 to 185.0 MJy sr^{-1} (white to black). (d) Original 100 μm HRES image. The beam shape is displayed in the lower right-hand corner. The image is scaled from 40.0 to 350.0 MJy sr^{-1} (white to black).

ing factor of the dust is only about 0.4–0.5 (see § 6.4). Furthermore, the total radio flux at 1420 MHz is lower than expected for an ionization bounded nebula surrounding VES 735, with a similar implied covering factor (§ 4.2.2). This together with geometrical information to be discussed (e.g., § 4.1) implies that KR 140 is a bowl-shaped H II region (cf. Roger & Irwin 1982) rather than a classical Strömgren sphere, a not unexpected morphology when the O star is close to the edge of its parent molecular cloud (Yorke, Tenorio-Tagle, & Bodenheimer 1983). This model is perhaps the simplest geometry that is consistent with the derived covering factors, but our data cannot rule out other, more complicated geometries, such as a broken shell or a shredded and dissipated Strömgren sphere. Observations of a champagne flow (Tenorio-Tagle 1979), perhaps via Fabry-Perot imaging, could help establish whether or not KR 140 is truly a blister region.

The circular symmetry observed in the dust shell (and in the ionized gas) implies that we are observing KR 140 almost face on (i.e., the opening of the bowl is oriented almost along the line of sight). For example, see the simulated radio maps of the R2 model by Yorke et al. (1983). The CO data and extinction measurements to VES 735 both suggest that the molecular cloud is behind the star, with the inferred opening toward us (§ 7.1).

4. KR 140 FROM THE PERSPECTIVE OF THE RADIO CONTINUUM

4.1. Size and Structure

The basic radio morphology appears to be that of a limb-brightened hemispherical shell (most of the free-free emis-

sion would be from the dense and thin ionization-bounded zone). The last contour shown (at $T_b = 5.0$ K) in Figure 3 has a diameter of 8.5, which for a distance $d = 2.3$ kpc corresponds to a physical diameter of about 5.7 pc. It is expected that neutral material could extend well beyond the H II region, and indeed there is both dust (§ 6.2) and CO gas (§ 7.1) around KR 140. The free-free surface brightness falls off most quickly (the radio contours are more tightly spaced) in the west-northwest part of the nebula. A sharper ionization front would occur in more dense (preexisting) material.

Other internal detail might be interpreted as variations in distance between the star and the background ionization front, with lower surface brightness features originating from sectors farther from the star; such an interpretation of radio surface brightness has been used to construct a topological map of the ionized surface of the Orion molecular cloud behind the Trapezium (Wen & O’Dell 1995). If we use the 1420 MHz surface brightness at the pixels near the projected position of VES 735 and the known properties of this O8.5 V exciting star, the distance that the star must be from the back of the nebula turns out to be only 2.14 pc. Together with the above estimate of the diameter across the line of sight, this is consistent with the idea that KR 140 is similar to a hollowed-out hemispherical bowl.

4.2. Physical Properties

In this section we use the 1420 MHz data to derive a number of physical properties of the nebula. For ease of reference, Table 1 summarizes these properties, some of the properties of the exciting star, and other quantities that we later derive from the infrared and CO data.

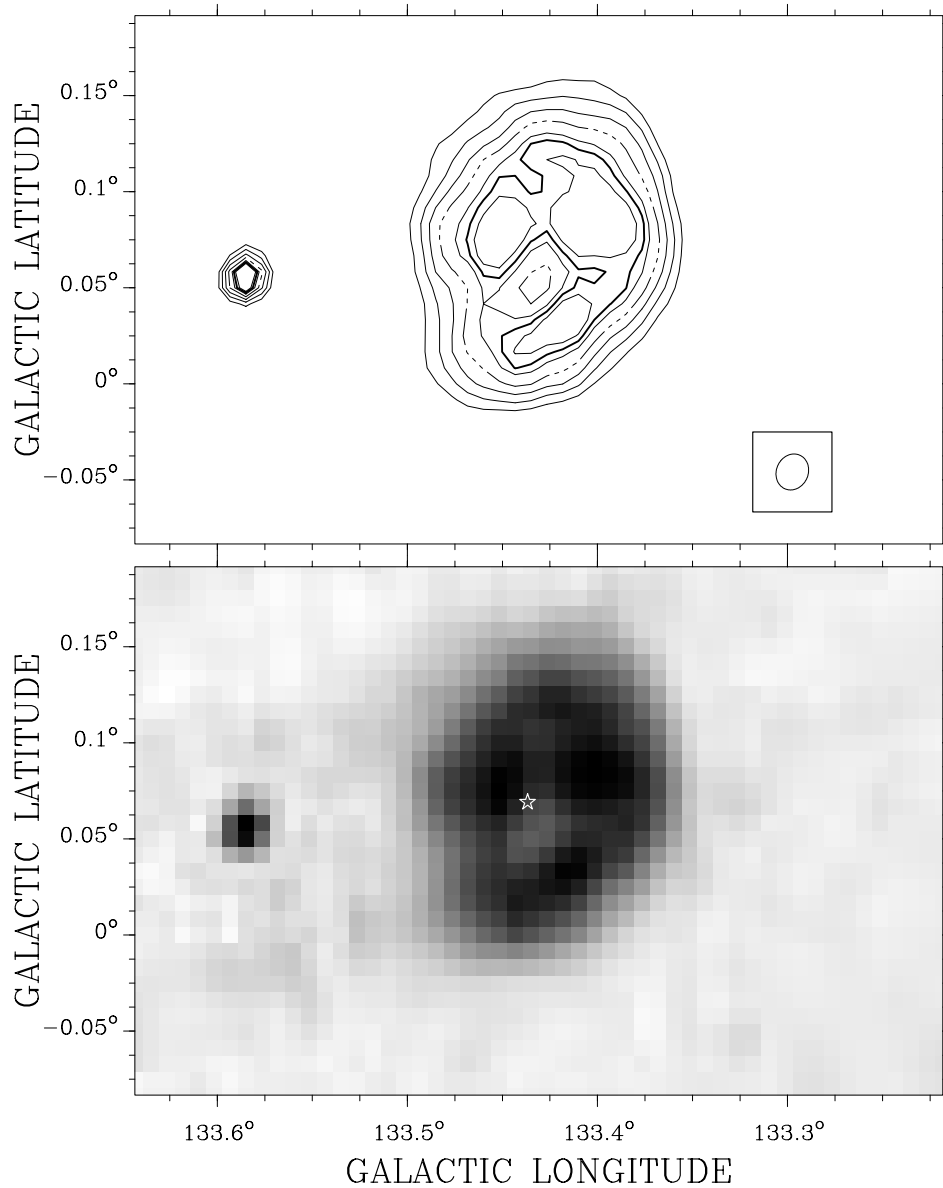


FIG. 3.—(Top) Contours of 21 cm brightness temperature of KR 140 at 5.0, 6.0, 7.0, 8.0 (dashed lines), 9.0, 9.5 (heavy lines), and 10.0 K. The source is slightly more extended than indicated by the lowest contour; the H II region fades into the background at contour level about 3 K. The beam shape is displayed in the lower right corner. (Bottom) Gray scale with linear brightness scale (1.868–11.0 K white to black). The point source at $l = 133^{\circ}585$ and $b = 0^{\circ}058$ is probably extragalactic as it has a nonthermal spectral index. The position of the exciting star of this region, VES 735, is denoted by the star.

4.2.1. Emission Measure, Radio Flux, Electron Density, and Ionized Mass

The KR 140 emission is optically thin at 1420 MHz with a peak brightness temperature about 10 K. For an optically thin nebula, the specific intensity (surface brightness) I_{ν} and brightness temperature $T_{b\nu}$ for thermal radiation are (Osterbrock 1989)

$$I_{\nu} \equiv 2\nu^2 k T_{b\nu} / c^2 = j_{\nu} \int n_i n_e ds \equiv j_{\nu} E, \quad (1)$$

where j_{ν} is the free-free emissivity, n_i is the ion density, n_e is the electron density, ds measures distance along the line of sight, and the integral E is called the emission measure. For j_{ν} of a pure hydrogen nebula (a good approximation; see § 4.2.2 for models that include ISM abundances), $E = 5.77 \times 10^2 T_{b\nu} (T_e / 7500 \text{ K})^{0.35} (\nu / 1420 \text{ MHz})^{2.1} \text{ cm}^{-6} \text{ pc}$. The peak emission measure in the map is about $6000 \text{ cm}^{-6} \text{ pc}$

and after background subtraction $\langle E \rangle = 2050 \text{ cm}^{-6} \text{ pc}$. After subtracting the local Galactic background we find the total flux ($F_{\nu} = \int I_{\nu} d\Omega$) to be $2.35 \pm 0.05 \text{ Jy}$ at 1420 MHz. This is in good agreement with the value $2.3 \pm 0.2 \text{ Jy}$ reported by Kallas & Reich (1980). Becker, White, & Edwards (1991) detected this H II region in a 6 cm survey with the NRAO 91 m. Their source, designated [BWE91] 0216+6053, had $F_{\nu} = 2.5 \text{ Jy}$. Using the same telescope and frequency, Taylor & Gregory (1983) and Gregory & Taylor (1986) record this source as GT 0216+608 in their survey; in their analysis they treated all sources as point sources and so find systematically low fluxes for extended nebulae like this (648 mJy for KR 140).

In the optically thin limit the theoretical expectation for the spectral index for thermal radiation (defined as $I_{\nu} \propto \nu^{\alpha}$) is $\alpha \approx -0.1$ (Oster 1961; Gordon 1988). The spectral index of KR 140 was measured between 1420 and 408 MHz. First,

TABLE 1
KR 140 PHYSICAL PROPERTIES

Property	Value
General	
Distance ^a (kpc)	2.3 ± 0.3
Diameter (pc)	5.7
Exciting Star ^a	
Name	VES 735
Apparent <i>V</i> magnitude	12.88 ± 0.01
Apparent <i>B</i> − <i>V</i>	1.53 ± 0.02
Spectral type	O8.5 V(e)
log [<i>Q</i> (H ⁰)]	~48.5
<i>L</i> _{bol} (<i>L</i> _⊙)	~10 ⁵
Radio Continuum (1420 MHz)	
Flux density (Jy)	2.35 ± 0.05
Average emission measure (cm ^{−6} pc)	2000
<i>n</i> _e (rms) (cm ^{−3})	30
<i>M</i> _{H II} (<i>M</i> _⊙)	160
log [<i>Q</i> (H ⁰)]	48.05 ± 0.1
Infrared (<i>IRAS</i>) ^b	
<i>F</i> ₁₂ (Jy)	110
<i>F</i> ₂₅ (Jy)	140
<i>F</i> ₆₀ (Jy)	970
<i>F</i> ₁₀₀ (Jy)	2300
<i>L</i> _{bol} (<i>L</i> _⊙)	10 ^{4.5}
Molecular Line (CO: <i>J</i> = 1–0)	
<i>n</i> _{H₂} (cm ^{−3})	~100
Current <i>M</i> _{total} (<i>M</i> _⊙)	4400

^a Data from Kerton et al. 1999.

^b Fluxes measured from HIRES images of KR 140.

the distribution across the nebula was determined using L. Higgs' SPECMAP routine (Zhang & Higgs 1997), which evaluates the spectral index for the spatially variable component of the emission (this approach has the advantage of circumventing uncertainties in background subtraction in each image); for this procedure, we convolved the 1420 MHz image to the lower resolution of the 408 MHz image. The typical value of α is 0.02 ± 0.08 . We confirmed this by measuring the total background-subtracted flux at 408 MHz as well. Considering there is a 10% uncertainty in the flux calibration in the 408 MHz pilot project data at the position of KR 140 (Taylor 1999), the derived spectral index is in satisfactory agreement with theory.

Depending on details of the geometry, the appropriate path length for estimating the density would be of order the observed radius; with this choice we find an rms $n_e = 27$ cm^{−3}. The mass of radio-observable ionized gas (allowing for He) is $163 (27 \text{ cm}^{-3}/n_e) M_{\odot}$. For comparison, the exciting star of KR 140 has a mass of $25 M_{\odot}$ (Kerton et al. 1999).

4.2.2. Number of Ionizing Photons

In ionization equilibrium the number of ionizations (where H is the predominant species) that occur each second in the nebula is equal to the number of (H⁺) recombinations each second, both locally and globally. An ionization-bounded nebula occurs when there is sufficient material to intercept all of the ionizing photons ($\lambda \leq 912 \text{ \AA}$), $Q(\text{H}^0)$, emitted by the star per second (Osterbrock 1989). Formally, the spatially integrated radio emission of an

ionization-bounded nebula is an effective calorimeter for $Q(\text{H}^0)$:

$$fQ(\text{H}^0) = \int n_e n_{\text{H}^+} \alpha_{\text{B}} dV = \alpha_{\text{B}} F_{\nu} d^2/j_{\nu}, \quad (2)$$

where α_{B} is the case B hydrogen recombination coefficient of H⁺ ($\approx 3.3 \times 10^{-13} \text{ cm}^3 \text{ s}^{-1}$ at 7500 K; Storey & Hummer 1995), dV is the volume element, and we have used $dV = ds d\Omega \times d^2$ and equation (1) to find the right-hand side. Here f is the product of a number of correction factors, including f_{ci} , the all-important covering factor by an ionization front: if the star is only partially surrounded by gas then a fraction of the ionizing photons will escape and a lower F_{ν} will result.

Equation (2) is based on recombination and emissivity for a pure H nebula at a fixed temperature, so f is made up of a number of factors that modify the expected radio continuum flux for a given $Q(\text{H}^0)$. We used the spectral synthesis code Cloudy (Ferland et al. 1998) to analyze the observations of KR 140 in the radio, particularly the correction factors that comprise f . We constructed a number of toy models for differential comparisons, using a 35,500 K blackbody with $\log [Q(\text{H}^0)] = 48.06$ and $n_e = 50 \text{ cm}^{-3}$; see Table 2. The differential results are appropriate for any low-density H II region heated by a late O-type star.

The temperature of the nebula enters in the equation through the α_{B} and j_{ν} factors, although the effect on the ratio is very small. Comparing models 1 and 6 we estimate $f_T = 0.99$.

The effect of the addition of other elements to the nebula is to increase the total radio flux. This effect is primarily due to the presence of He⁺ increasing the effective free-free emissivity (He has a tiny effect on the amount of ionization of H; e.g., Osterbrock 1989). Comparing models 1 and 4 or models 2 and 5 we estimate that $f_{\text{He}} = 1.07$.

Dust competes with the gas for the absorption of ionizing photons and thus, when present in the nebula, will reduce the observed radio F_{ν} for a given $Q(\text{H}^0)$. Comparing models 1 and 2 (with grains) to model 3 (without grains) we derive $f_{\text{dust}} = 0.78$ for the typical ISM grains used in model 2 and $f_{\text{dust}} = 0.93$ for dark-cloud dust, similar to the dust found in Orion, used in model 1. The dark-cloud dust is not as efficient as typical ISM dust in absorbing short-wavelength photons and so has less of an effect on the emergent radio flux.

The combination of these factors, except for the covering factor, leads to a factor of $f_{\text{model}} = 0.91 \pm 0.08$ depending upon the grain composition (i.e., $f = 0.91f_{\text{ci}}$).

In our study of the exciting star VES 735 (Kerton et al. 1999) we used the measured radio flux at 1420 MHz

TABLE 2
RADIO FLUX FACTORS

Model	Abundance ^a	Grains ^b	Temperature	νF_{ν} (ergs s ^{−1} cm ^{−1})
1	H II	Orion	Variable	4.2
2	H II	ISM	Variable	3.6
3	H II	None	Variable	4.6
4	No He	Orion	Variable	3.9
5	No He	ISM	Variable	3.3
6	H II	Orion	Fixed (7500 K)	4.3

^a H II = average H II abundance as reported by Ferland 1996.

^b ISM = typical high-*R* grains; Orion = low-*R* grains; see Ferland 1996 for details.

(2.35 ± 0.05 Jy) to calculate $\log [fQ(H^0)] = 48.05 \pm 0.11$ and then estimated $f_{\text{ci}} \approx 0.4\text{--}0.5$ based on the known spectral type of VES 735 (O8.5 V(e); $\log [Q(H^0)] \sim 48.45$; Panagia 1973). We have not attempted to put any formal error estimate on the covering factor, but given the uncertainties involved, both in the stellar properties and in estimating the various f factors, this result is certainly consistent with the idea of KR 140 being an open bowl-shaped region. As demonstrated in § 6.4, an analysis of the IR data leads to the same conclusion independently.

5. THE AGE OF KR 140

The approach we have adopted here is first to date the H II region using data we have on the exciting star VES 735. With that age in mind, we then investigate the dynamics of the region, the goal being to show that certain scenarios for the evolution of KR 140, such as it being a blister region, are at least consistent with the age suggested from the exciting star. This approach is similar to that adopted by Dorland, Montmerle, & Doom (1986) in their study of the Rosette Nebula.

5.1. Stellar Content

The idea of using the stellar content of a H II region to measure the age of the nebulosity was first attempted by Hjellming (1968). Basically one plots the evolutionary tracks of stars with various masses in the $\log(L/L_\odot)$ versus $\log T_{\text{eff}}$ plane. One obtains T_{eff} from the spectral type of the exciting star and $\log(L/L_\odot)$ from the radio flux [much like $Q(H^0)$], and then the position in the plane determines an age for the star and thus the H II region. Clearly the effectiveness of this technique depends strongly on the quality of the calibration between theoretical and observational quantities as well as the quality of stellar models, which have vastly improved in the 30 years since this technique was introduced. In the early work the primary result was to indicate whether the H II regions were ionization or density bounded and that many H II regions required additional, unobserved, sources of ionization.

Here we follow a technique slightly different from that of Hjellming (1968) in order to avoid any uncertainties associated with the covering factor and structure of the nebula. We instead use the absolute magnitude (M_V) as a measure of $\log(L/L_\odot)$, which is possible because we have a good estimate of the distance to the star and the extinction along the line of sight (Kerton et al. 1999). Figure 4 plots the stellar evolution models of Schaerer & de Koter (1997) for 20, 25, and 40 M_\odot stars along with the value determined for VES 735. The observed values for VES 735 are consistent with a 25 M_\odot star with an age of a few million years away from the zero-age main sequence (ZAMS; see Fig. 4), where the age would be only of order 10^5 yr. Of course, the spectral type alone gives us a simple upper limit to the age of KR 140: for an O8.5 V star the main-sequence lifetime is $\sim 6 \times 10^6$ yr (Chieffi, Limongi, & Straniero 1998).

5.2. Dynamical Models: Spherically Symmetric

5.2.1. Strömgen Sphere

The simplest description of a H II region is that of the formation and expansion of an ionized ball of pure hydrogen at constant temperature in a uniform medium of constant density (Strömgen 1939). We summarize this only as a point of departure and contrast. The evolution of a Strömgen sphere starts with a formation phase where the

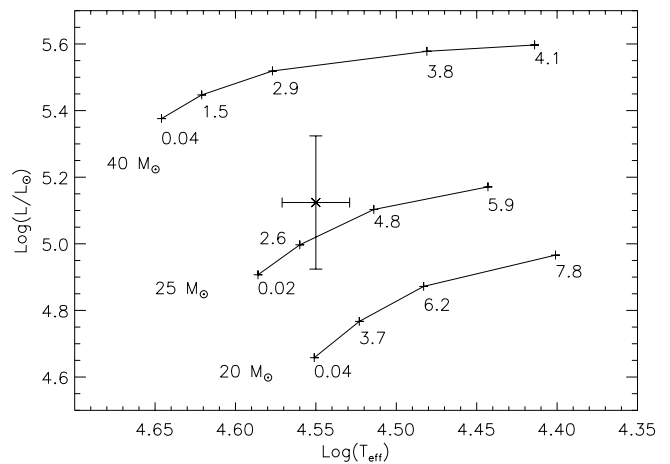


FIG. 4.— $\log(L/L_\odot)$ vs. $\log T_{\text{eff}}$ with evolutionary models of Schaerer & de Koter (1997) shown for three high-mass stars. Individual points in the models (crosses) are labeled with the stellar age (10^6 yr). The point with error bars represents VES 735, the exciting star of KR 140.

O star ionizes a region of space around it to the radius (R_s) given by

$$R_s = \left[\frac{3Q(H^0)}{4\pi n_e^2 \alpha_B} \right]^{1/3}. \quad (3)$$

The initial rapid expansion to a radius of r_i occurs in time $t = (-1/n_e \alpha_B) \ln [1 - (r_i/R_s)^3]$ (valid to $r_i/R_s \sim 0.98$; Osterbrock 1989). The time to create the initial Strömgen sphere is about $10^5/n_e$ (cm^{-3}) yr, instantaneous compared to other timescales. For KR 140, the observed radius (R_{obs}) is 2.85 pc. Taking $\log [Q(H^0)] = 48.45$ for an O8.5 V(e) star like VES 735 (Panagia 1973) and $n_{\text{H}_2} = 100 \text{ cm}^{-3}$ for the original molecular cloud, $R_s = 1.2$ pc. The initial H II region is overpressured compared to the surroundings and will expand into a uniform medium according to a $t^{4/7}$ law:

$$r_i/r_o = \left(1 + \frac{7C_{\text{II}} t}{4r_o} \right)^{4/7}, \quad (4)$$

where C_{II} is the sound speed in the ionized medium, r_o is the initial radius and r_i is the radius at time t . With the densities quoted above the H II region will evolve from R_s to R_{obs} on a timescale of 10^5 yr, which is improbably short. Increasing the initial density makes R_s smaller and forces the pressure expansion stage to be longer. A value of $n_{\text{H}_2} = 500 \text{ cm}^{-3}$ will push the timescale to 10^6 yr. However, this value is not consistent with our observations of the molecular material (§ 7), so the Strömgen sphere is not an appropriate dynamical model for KR 140.

5.2.2. Stellar Winds

In the radio image a local minimum is evident near the position of the central star (see Fig. 1 in Kerton et al. 1999). One interpretation is that this is a wind blown bubble around the O8.5 V(e) star. The apparent radius of the central hole is 1.4 pc. We used the model of Castor, McCray, & Weaver (1975) for the size of a circumstellar shell:

$$R = 28 \left(\frac{\dot{M}_6 V_{2000}^2}{n} \right)^{1/5} t_6^{3/5} \text{ pc}, \quad (5)$$

where R is the shell's radius (pc), \dot{M}_6 is the mass-loss rate ($10^{-6} M_\odot \text{ yr}^{-1}$), V_{2000} is the wind velocity (2000 km s^{-1}), n

is the gas density (cm^{-3}), and t_6 is the time (10^6 yr). Stellar wind properties of the B2 model of Schaerer & de Koter (1997) were used. For a wide range of densities we obtain timescales on the order of only 10^4 yr. This is far too low a timescale, and clearly this model is not an appropriate description of VES 735. Either the mass-loss rate adopted is much too high or the assumption of spherical symmetry is not valid.

5.3. Dynamical Models: Open Geometry

Evidence summarized thus far (§§ 4.2.2 and 6.4) indicates an open geometry with a covering factor of about 0.5 for both dust and ionized material. In this case the high pressure in the interior of the initial Strömgren sphere or stellar wind bubble is relieved, slowing down the expansion. Models have been developed to investigate the evolution of an H II region at the edge of a molecular cloud (see review of early models by Yorke (1986), and Comerón (1997) for a recent example). While complex numerical modeling is possible, Franco, Shore, & Tenorio-Tagle (1994) have shown that the expansion of the ionization bounded side of such a blister H II region is well described by

$$r_i/r_o = \left(1 + \frac{5C_{\text{II}}t}{2r_o}\right)^{2/5}. \quad (6)$$

This is based upon mass conservation between material being ejected in the flow and molecular material being eroded off the cloud. One can envisage the evolution of a blister as consisting of three stages: the initial rapid formation stage, a pressure-driven expansion stage, and finally a blow-out stage. The relative length of time of the latter two stages depends upon the distance of the star from the edge of the cloud and the density structure of the cloud. One very important point is that an O star very close ($\sim 1R_s$) to the edge of a cloud will very quickly develop a covering factor of ~ 0.5 in order 10^5 yr and will maintain this covering factor over the lifetime of the O star (Yorke et al. 1983, 1989). We assume that the star formed very close to the edge of the cloud, thus ignoring the pressure-driven expansion stage. Using equation (6), the age of the region is of order 10^6 yr when $R_s = 0.64$ pc. For the stellar properties of VES 735 this requires $n_{\text{H}_2} \sim 280 \text{ cm}^{-3}$. This is somewhat encouraging as it does not require as vast a difference between the properties of the observed molecular cloud and the putative initial conditions.

6. KR 140 IN THE INFRARED

6.1. Morphology and Emission Mechanisms

Stars that are forming and evolving in the ISM interact with the interstellar dust component by heating, redistributing, and possibly destroying it. The dust can be heated by at least three distinct mechanisms: direct radiation from the central star, reprocessed radiation from the ionized gas, and diffuse radiation from the interstellar radiation field. Radiation pressure from the star acts on the dust in the ionized zone (Spitzer 1978), which causes the dust (and gas) to be pushed away from the star. Some forms of dust like polycyclic aromatic hydrocarbons (PAHs) are destroyed in intense ultraviolet fields. A morphological study of the infrared emission from KR 140 is therefore important to fully understand the energetics and effects on the environment.

As mentioned in § 2, *IRAS* scans of KR 140 at 12, 25, 60, and 100 μm were processed by the HIRES software to generate maps of about $1'$ resolution. The new beam shapes are somewhat elliptical, so point sources will be visibly stretched; however, the larger scale morphology of the observed dust emission from the nebula will not be greatly affected by the asymmetric beam.

The intensity of the dust emission, I_{dust} , at a particular frequency, ν , from a distance increment ds along the line of sight has the form

$$I_{\text{dust}} = N_{\text{dust}} \pi a^2 B_{\nu}(T_{\text{dust}}) Q_{\nu}(a, T_{\text{dust}}) ds, \quad (7)$$

where N_{dust} is the number density of grains, $B_{\nu}(T_{\text{dust}})$ is the Planck function at a temperature T_{dust} , a is the radius of the particles, and $Q_{\nu}(a, T_{\text{dust}})$ is the absorption efficiency factor.

Figure 2 shows the four HIRES images of KR 140, with the 12 and 25 μm images convolved to the 1420 MHz resolution, and overlaid by 1420 MHz contours (Figs. 2a and 2b). The 12 and 25 μm emission is spread well outside the radio contours of KR 140 (this is taken up in § 6.3). Features that are common to all four images in Figure 2 are the bright arcs on either side of the nebula (easiest to see in Fig. 2c) that extend outside the radio contours. We interpret this as the limb-brightened warm dust shell around KR 140. Note that there could be cooler dust farther out around the KR 140 complex that will not have been detected in the *IRAS* bands. We account for the energetics of this cooler dust in our models of KR 140 (§ 6.4).

6.2. Temperature and Column Density

Equation (7) can be used to calculate a mean dust temperature for each pixel of IR emission. Taking the intensity ratio for any two frequencies, ν_1 and ν_2 , yields

$$\frac{I_{\nu_2}}{I_{\nu_1}} = \left(\frac{\nu_2}{\nu_1}\right)^{3+\beta} \left(\frac{e^{h\nu_1/kT} - 1}{e^{h\nu_2/kT} - 1}\right), \quad (8)$$

where T is the T_{dust} of equation (7) and the $(\nu_2/\nu_1)^{3+\beta}$ factor is from the frequency-dependent part of $Q_{\nu}(a, T)$, where β depends on the type of dust. The most common components proposed for interstellar dust are silicate and graphite (or some related carbonaceous material), which, at long wavelengths, have $\beta \approx 2$. This value of β is close to what is generally observed in the ISM (Lagache et al. 1998).

The 60 and 100 μm data were used to calculate the dust temperature map, as they are the bands where classical grain emission dominates. It is likely that nonequilibrium heating of very small dust grains (VSGs) contributes some of the observed 60 μm flux, so the derived temperatures are probably slight overestimates of the true grain temperatures (Boulanger, Baud, & van Albada 1988). The images were brought to the same resolution and background subtracted, and the IPAC analysis program CTTM was used to compute a dust temperature map. An azimuthally averaged radial cut of this map is shown in Figure 5. The temperature distribution was sampled every $1'$ in radius and every 10° azimuthally. The temperatures in the central region are around 31 K. Nearer the edge of the H II region, the dust temperatures drop to around 28 K. However, a line of sight passing near the star also has cooler dust in the background and the foreground, which would lower the apparent temperature observed.

A calculation of dust temperature from first principles was done as a check on the empirical values output from

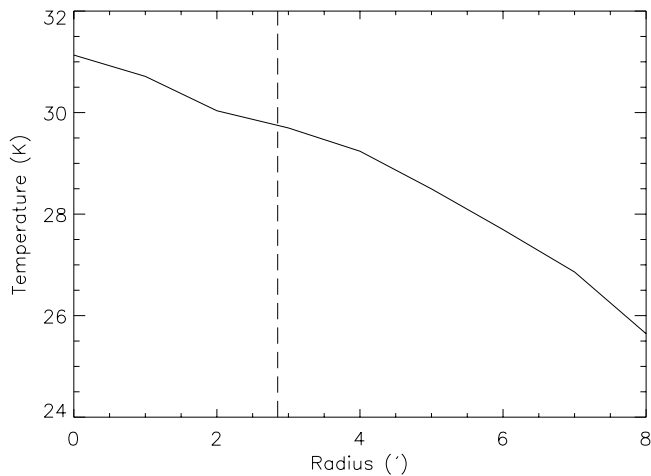


FIG. 5.—Azimuthally averaged dust temperature profile for KR 140. Origin is located at $l = 133^{\circ}43$, $b = 0^{\circ}068$. The extent of the ionized region is indicated by the dashed vertical line. The temperature distribution was sampled every $1'$ in radius and every 10° azimuthally.

CTTM. In this calculation, a single silicate or graphite dust grain with a radius of $0.1 \mu\text{m}$ (a typical interstellar size; see Kim, Martin, & Hendry 1994) was placed at a distance of 3.0 pc from the center of the nebula, corresponding to a dust grain within the KR 140 dust shell. The luminosity of the O8.5 V(*e*) exciting star is about $10^5 L_{\odot}$ (Panagia 1973). Making use of Planck-averaged absorption factors from Laor & Draine (1993), we find that if $\tau_{\text{UV}} \approx 1$, the calculated dust temperature is about 28 K , in agreement with the temperature deduced empirically. Note, however, that this calculation did not take into account the recombination-line photons emitted by the ionized gas. Furthermore, some of the free-free photons and collisionally excited cooling lines are emitted not in the ultraviolet, but in the optical

(Osterbrock 1989), where the dust absorption efficiency is somewhat lower.

The optical depth τ_{ν} from dust is defined to be

$$\tau_{\nu} = \int N_{\text{dust}} \pi a^2 Q_{\nu}(a, T_{\text{dust}}) ds \quad (9)$$

and can be calculated by dividing I_{ν} (eq. [7]) by the Planck function $B_{\nu}(T)$, assuming a constant T along the line of sight, adopted from the temperature map. Figure 6 displays a dust optical depth map at $100 \mu\text{m}$. The values range from about 0.0004 in the middle of the nebula to about 0.002 in the bright northwest rim. These values show that the dust is transparent to its own $100 \mu\text{m}$ emission. The minimum in the center of the nebula and the ring-shaped appearance is most simply interpreted as limb brightening in a thick shell of dust with the highest column density along the northwest rim. The latter is the same region of the nebula where the 1420 MHz radio contours fall off most steeply (§ 4.1), and where there is no CO emission (§ 7.1).

The optical depth in the ultraviolet τ_{UV} can be gauged using extinction curves from the literature. We are interested in the radial as opposed to line of sight optical depth. Judging the thickness of the shell from one of the arcs in Figure 6 gives a path length of about $7 \times 10^{18} \text{ cm}$. If we assume the dust is associated with gas at a molecular density of 100 cm^{-3} , the molecular column density of this gas is about $7 \times 10^{20} \text{ cm}^{-2}$. Using the extinction curves of Kim et al. (1994), we find that $\tau_{\nu} \approx 2.8$ at 1100 \AA (far in the ultraviolet), whereas at 5500 \AA (in the optical), $\tau_{\nu} \approx 0.6$. The estimated optical depths show that the dust in the arcs has a high enough radial optical depth to absorb most of the incident ultraviolet photons. However, since KR 140 has a covering factor of $0.4\text{--}0.5$ (§§ 4.2.2 and 6.4), the total infrared luminosity of the nebula will be correspondingly less than the bolometric luminosity of VES 735 (§ 6.4).

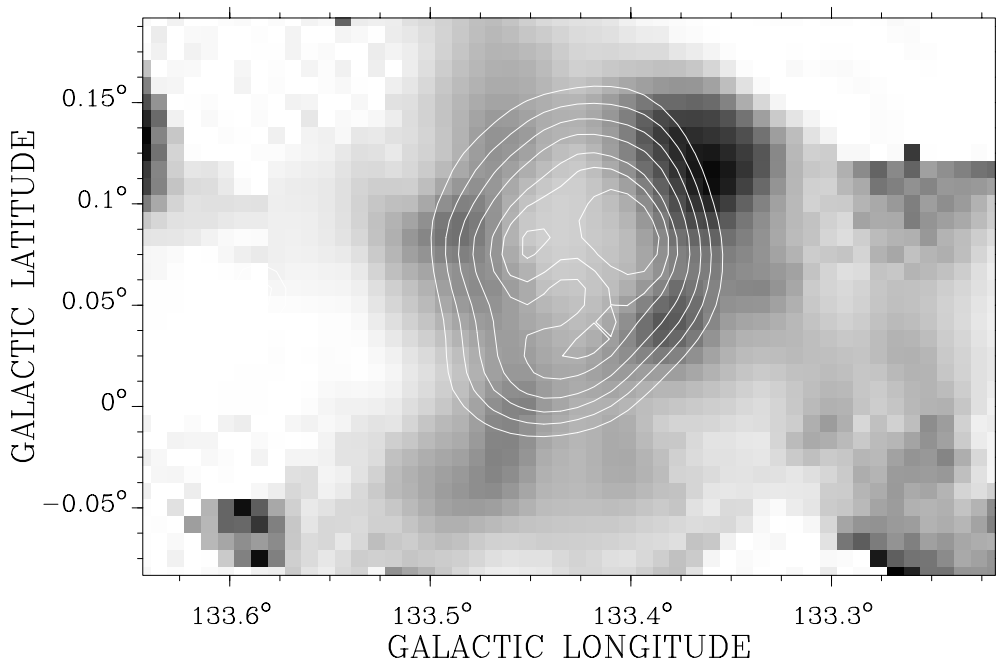


FIG. 6.— τ_{100} map overlaid with the 1420 MHz contours. The gray scale is linear with a white value of 0.0 and a black value of 0.002 . Both images and the contours are at the $100 \mu\text{m}$ resolution.

6.3. The 12 and 25 μm Emission

It has been known for over a decade that there is excess emission within the 12 μm *IRAS* passband (e.g., Boulanger et al. 1985). Onaka et al. (1996) found that more than 70% of the 12 μm diffuse interstellar emission detected by *IRAS* is emitted in spectral features attributed to polycyclic aromatic hydrocarbons (PAHs; Léger & Puget 1984; Allamandola, Tielens, & Barker 1985). The 12 μm image of KR 140 is very instructive. There is very little 12 μm flux within the radio contours of KR 140, implying that PAHs are destroyed there in the intense ultraviolet radiation field. However, there is a large amount of diffuse flux outside the radio contours, especially to the west (Fig. 2a). The PAH emission is a tracer of the photodissociation region around a nebula (Giard et al. 1994; Bregman et al. 1995; Fig. 10).

Unique among the HIRES images of KR 140, the 25 μm image (Figs. 2b and 7) shows a bright spot near the center of the nebula, on a transition between a radio peak (the “left eye”) and the deepest depression. The *IRAS* Point Source Catalog (Joint *IRAS* Science Working Group 1988) lists this feature as IRAS 02165+6053, and it also has been identified with VES 735 (Bidelman 1988). Figure 7 shows that IRAS 02165+6053 and VES 735 are practically coincident. Dust closer to the star would tend to be warmer, contributing to the spot if not pushed away by radiation pressure.

The entire nebula looks hotter and more extended at 25 μm than it would be for equilibrium emission from normal-sized grains. Most of the 25 μm emission is probably contaminated by nonequilibrium emission from very small grains (VSGs; Sellgren 1984) that have absorbed a UV photon and have had their temperatures instantaneously rise to $\sim 10^3$ K. Although these small grains make up a tiny fraction of the mass in the dust distribution, they make up a good fraction of the number distribution and absorb a significant fraction of the near-ultraviolet radiation. This VSG

emission is therefore a major source of uncertainty when analyzing the 25 μm image.³ Note that the “temperature-spiking” phenomenon also occurs outside the ionized zone, far from the exciting star.

6.4. Infrared Models

H II regions are some of the most luminous objects in the Galaxy when observed in the infrared, especially at wavelengths longer than 60 μm . In fact, if the dust shell covers 4π steradians around the exciting star, the infrared luminosity should be a good measure of the star’s bolometric luminosity. To account for the true extent of the dust, we can define a covering factor of dust (f_{cd}). Often it is simply assumed that $L_{\text{IR}} = L_{\text{bol}}$; however, this is not correct even for $f_{\text{cd}} = 1$. Some of the radiation from the star and nebula is at long enough wavelengths to avoid being absorbed by the dust. Using Cloudy we found that, for models with $f_{\text{cd}} = 1$, $\log(L_{\text{IR}}/L_{\text{bol}}) \sim -0.1$.

To calculate the integrated infrared flux from KR 140, the background in each of the four HIRES images was fitted and subtracted, and the total flux from the nebula was measured in each band. In order to estimate L_{bol} using these data, we used Cloudy to simulate the emission from large classical grains, roughly matching the fluxes at 60 and 100 μm . This approach allows us to account for emission from grains with a range of temperatures and thus unobserved emission at long wavelengths. First, we constructed models with $f_{\text{cd}} = 1$. We find $\log(L_{\text{FIR}}) = 37.90$. Since the resulting spectrum misses most of the observed 12 and 25 μm flux (which is caused by temperature spiking of VSG’s and the excitation of PAH molecules), we converted the observed 12 and 25 μm fluxes to luminosities using top-hat approx-

³ Further evidence for contamination in the 25 μm *IRAS* passband was presented by Cox (1990). He suggests that an iron oxide emission line falls within this *IRAS* passband, which would result in even greater excess 25 μm emission.

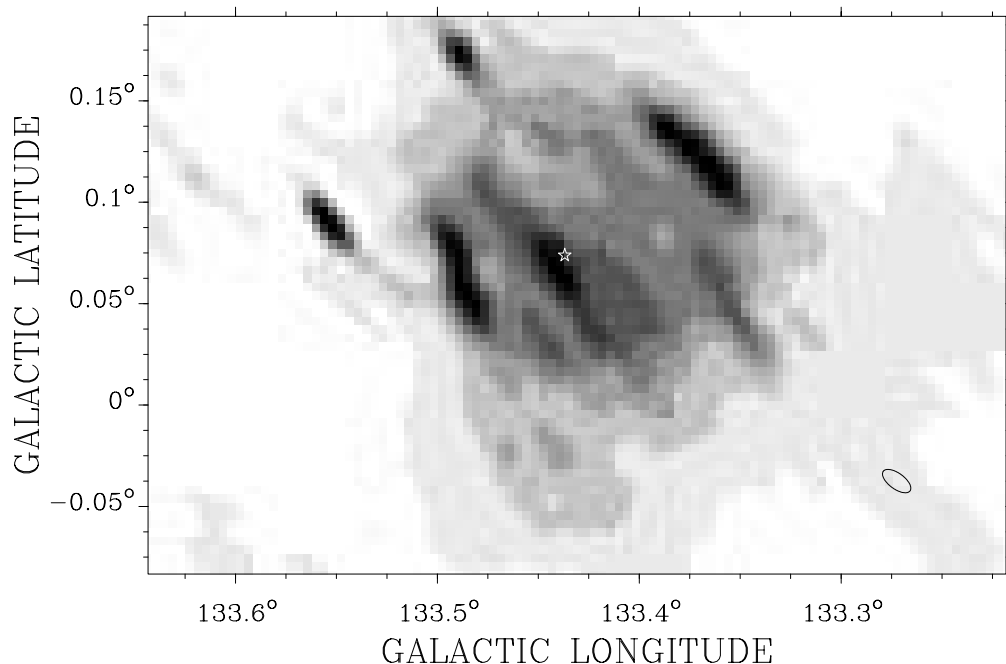


FIG. 7.—HIRES image of KR 140 at 25 μm . The gray scale is linearly spaced with a white value of 4.0 MJy sr^{-1} and a black value of 30.0 MJy sr^{-1} . The star near the center of the nebula corresponds to the position of the ionizing star VES 735. The beam shape of this HIRES map is shown in the lower right-hand corner.

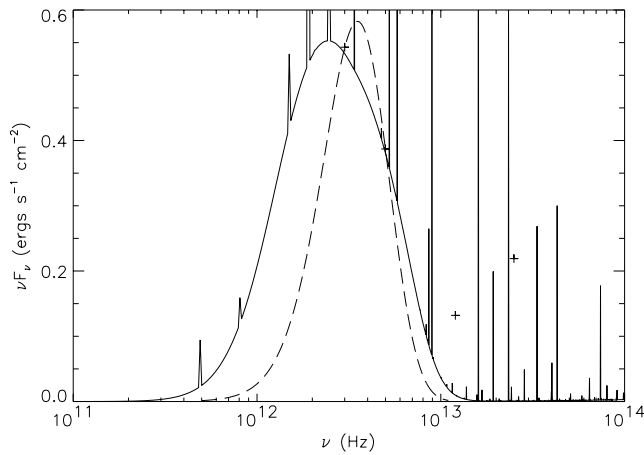


FIG. 8.—Cloudy model (*solid line*) using VES 735 stellar parameters and $f_c = 0.44$. Integrated *IRAS* fluxes for KR 140 are shown by the crosses. A single-temperature (28.25 K) $\nu^2 B_\nu$ spectrum is shown for contrast (*dashed line*).

iminations to the *IRAS* passbands (Emerson 1988) and added the results to L_{FIR} . With this addition we find $\log(L_{\text{IR}}) = 38.00$. Correcting from L_{IR} to L_{bol} we find $\log(L_{\text{bol}}/L_\odot) = 4.52$. This is significantly below what would be expected for any late O main-sequence star (e.g., Panagia 1973). We interpret this low apparent L_{bol} as being due to a covering factor of 0.4–0.5.

We know that VES 735 is an O8.5 V(e) star. Figure 8 demonstrates that one can reproduce the observed L_{IR} using the appropriate stellar parameters and a covering factor of about 0.5. A single-temperature ($T = 28.25$ K) $\nu^2 B_\nu$ spectrum is shown for comparison; note the wider model curve caused by the range of dust temperatures contributing to the emission.

Using an alternative calibration of stellar parameters that includes wind-blanketed models (Kerton 1999), we find $f_{\text{cd}} \sim 0.5$ and $f_{\text{ci}} \sim 0.7$. These results are still consistent with a blister model for KR 140.

7. KR 140 IN A MOLECULAR CLOUD

7.1. CO Signature

A slit spectrum of VES 735 allowed us to measure the radial velocity of the nebular H α line within 30" of VES 735 to be -46 ± 2.1 km s $^{-1}$ with respect to the local standard of rest (LSR) (Kerton et al. 1999). The differential radial velocity between VES 735 and the nebular line was measured to be $+2.0 \pm 2.2$ km s $^{-1}$.

An expected effect of the evolution of the H II region is photodissociation of molecular gas both inside the H II region and in the immediate surrounding interstellar medium (ISM). The CO data traces the molecular gas content of the ISM, so an examination of the CO data cube ought to reveal a lack of emission near the ionized gas velocity of KR 140. Indeed, a distinct CO hole was found within the radio contours of KR 140 over the velocity range -45.53 km s $^{-1}$ to -47.16 km s $^{-1}$ (LSR), which corresponds to three channels of width 0.813 km s $^{-1}$ in the CO cube. At more negative velocities, CO emission from the parent molecular cloud fills in the 1420 MHz contours.

Figure 9 shows the sum of these three channels overlaid with the 1420 MHz continuum contours. A well defined ring structure is clearly seen. Interestingly, the ring does not extend all the way around the nebula: there is no CO emission in the northwest. This is the same area where the 1420 MHz contours are falling off more sharply (§ 4.1) and where there is a bright infrared arc (§ 6.1) and a bright H I feature (§ 8). The relationship between 12 μ m emission, which is a good tracer of the photodissociation region (PDR), and the CO emission is shown in Figure 10. The northwest peak in the 12 μ m emission corresponds to the region where there is

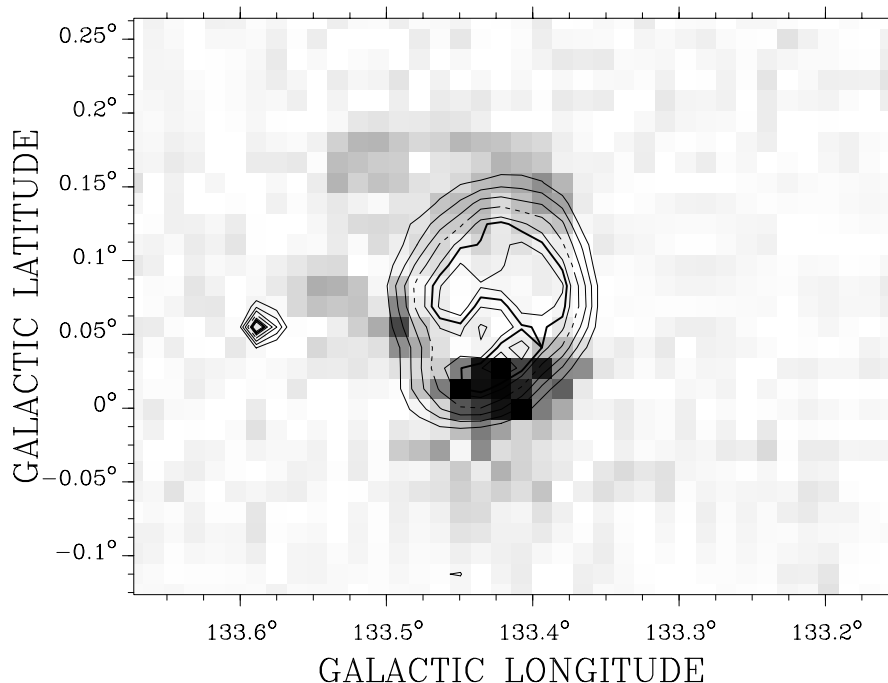


FIG. 9.—Image of integrated CO emission between -45.53 km s $^{-1}$ and -47.16 km s $^{-1}$ (LSR). 1420 MHz contours are overlaid with values that are the same as in Fig. 3. The image is linearly scaled from 0.0 to 15.0 K (*white to black*).

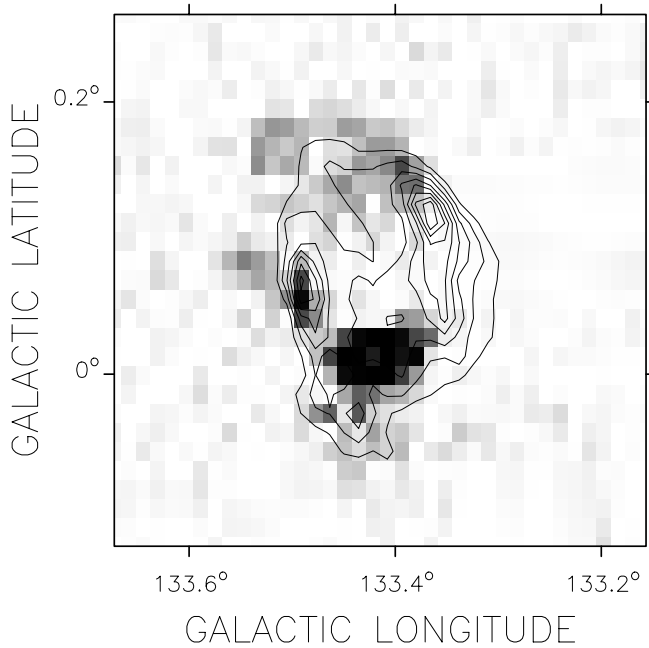


FIG. 10.—Integrated CO emission (-45.53 to -47.16 [LSR]) associated with KR 140 with contours of HIREs $12\ \mu\text{m}$ emission, both at $\sim 1'$ resolution. The CO image is linearly scaled from 0.5 to 10.0 K (white to black), and the contours are spaced $2\ \text{MJy sr}^{-1}$ apart from 7.0 to 25.0 MJy sr^{-1} .

no CO emission. To the east, as one moves away from the H II region, the $12\ \mu\text{m}$ peak occurs first followed by the peak in the CO emission.

7.2. Density and Mass of the Molecular Cloud

To estimate the mass of the molecular cloud, we integrated the CO cube over the whole velocity range of the cloud ($-45.5\ \text{km s}^{-1}$ to $-52.8\ \text{km s}^{-1}$) and measured the total surface brightness of the molecular cloud. We can use the empirical X factor to convert from CO surface brightness to molecular hydrogen column density. We have used $X = (1.9 \pm 0.5) \times 10^{20}\ \text{cm}^{-2}\ (\text{K km s}^{-1})^{-1}$ (Strong & Mattox 1996), where the quoted uncertainty is to take into account the range of X values measured for a variety of different clouds, to obtain a mean column density of $N(\text{H}_2) = 2.2 \times 10^{21}\ \text{cm}^{-2}$. Assuming a path length of 7 pc (the north-south radial extent), we find that the density of the molecular cloud is roughly $n_{\text{H}_2} = 100\ \text{cm}^{-3}$, typical of a giant molecular cloud (Blitz 1993).

By integrating the column density over the face of the cloud, we estimate the mass of the cloud to be $(4.4 \pm 1.6) \times 10^3\ M_\odot$. This mass includes an He correction factor of 1.36, and the error bar includes the distance uncertainty. The CO images show that the parent molecular cloud of KR 140 has been greatly disrupted by the nebula and the exciting star VES 735, so this mass will be an underestimate of the cloud's initial mass.

7.2.1. Estimating the Mass of the Original Molecular Cloud

One way to estimate the mass of the original molecular cloud would be to assume that KR 140 is indeed a blister H II region, as our data suggests. Yorke et al. (1989) have modeled blister H II regions with one exciting O star and found that mass-loss rate of material through the blister is $3\text{--}5 \times 10^{-3}\ M_\odot\ \text{yr}^{-1}$. However, these authors modeled an

O6 star in a cloud with $n_{\text{H}_2} = 500\ \text{cm}^{-3}$, which is not an accurate description of either VES 735 or its parental cloud. Unfortunately, Yorke et al. (1989) give no indication of how to scale their mass-loss rate for different values of $Q(\text{H}^0)$ or n_{H_2} . A analytic estimate of the amount of mass lost from a blister H II region is given by Whitworth (1979). His equation (41) has the desirable property that it agrees with the results of Yorke et al. (1989) for the values used in their models; therefore, it might have the correct scaling for $Q(\text{H}^0)$ and n_{H_2} . However, his calculations were based on a cylindrical geometry, which is not a very realistic model for a more bowl-shaped spherically symmetric region such as KR 140.

In § 5.3, we made use of the blister evolution formula given by Franco et al. (1994). These authors considered a simple symmetric blister region and were also able to estimate the cloud evaporation rate:

$$\dot{M} \approx \pi R_S^2 m_p 2n_{\text{H}_2} C_{\text{II}} \left(1 + \frac{5C_{\text{II}} t}{2R_S}\right)^{1/5}, \quad (10)$$

where R_S is the Strömgen radius and m_p is the proton mass. In § 5.3, we found that an initial cloud density of $280\ \text{cm}^{-3}$ and $R_S = 0.64\ \text{pc}$ would match the observed radius of KR 140 in a time of 1 Myr (consistent with the age of VES 735). Using these values in the above equation gives a mass-loss rate of $2.9 \times 10^{-4}\ M_\odot\ \text{yr}^{-1}$. Therefore, about $290\ M_\odot$ of molecular material has been eroded from the cloud after 1 Myr. Including the effects of dust lowers R_S , increases the age, and lowers \dot{M} , resulting in a very similar amount of erosion ($280\ M_\odot$).

Taking into account the mass lost through erosion and the present ionized mass, we estimate the mass of the original molecular cloud in which VES 735 formed to have been about $4.9 \times 10^3\ M_\odot$, so this cloud would be classified as a dwarf molecular cloud (Elmegreen 1985). This seems to be a remarkably small cloud mass for the formation of an O star. Williams & McKee (1997) performed a statistical analysis of many nearby OB associations and molecular clouds and found that it was more likely that clouds with masses greater than $10^5\ M_\odot$ should form O stars than clouds with lower masses. Other H II regions have been found with small molecular cloud masses (Hunter, Thronson, & Wilton 1990), but O star formation with a cloud mass below 10^4 is considered rare (Elmegreen 1985). Of course we have been attracted to this cloud because of the effect of VES 735 and not to other parts of the W3 cloud complex (Heyer et al. 1998) that have not formed O stars.

7.3. Interpretation of the Velocity

Stepping through the velocity channels in the CO data cube near the velocity of KR 140 shows that at higher (least negative) velocities ($\sim -40\ \text{km s}^{-1}$) there is no emission, then the CO emission comes in at the southern end of the H II region and spreads northward before filling in the 1420 MHz contours at a velocity of $-48.78\ \text{km s}^{-1}$. Perhaps the best way to illustrate these data is by examining the cube in velocity-latitude space. Figure 11 shows such a CO image of KR 140, averaged over the longitude range $133^\circ 366$ to $133^\circ 477$. Note the “hole” at the velocity of the ionized gas and VES 735.

The question arises as to the relative radial position of VES 735 and KR 140 with respect to the molecular gas. In general, it is difficult to use only the CO radial velocity

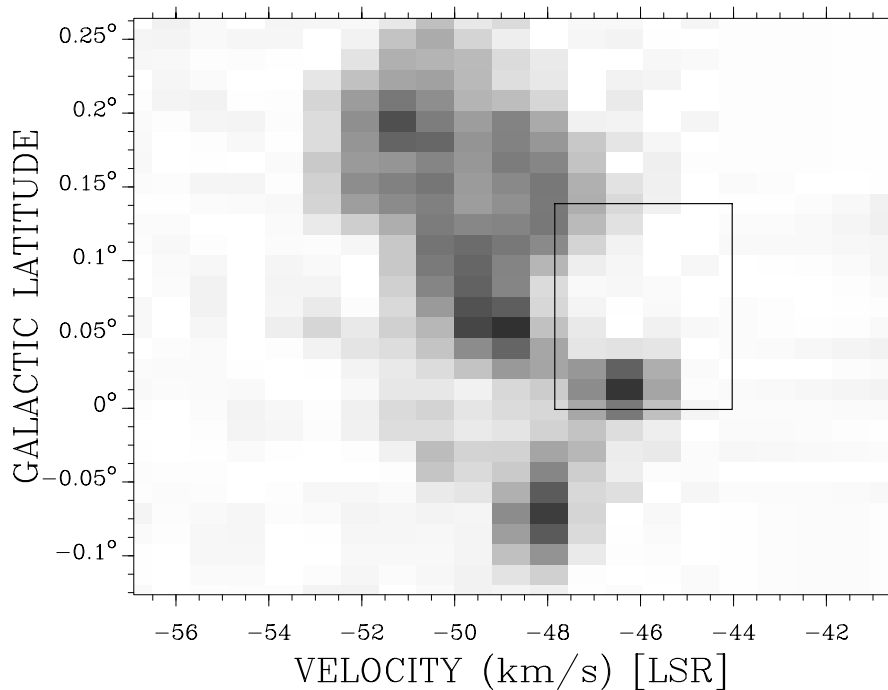


FIG. 11.—Velocity-latitude CO image of KR 140 averaged over the range $133^{\circ}366 < l < 133^{\circ}477$. The image is linearly scaled from 0.0 to 7.0 K (white to black). The rectangle denotes the area where the ionized gas is thought to reside. The latitude range was derived from the radio continuum image, and the velocity range is derived from the measured radial velocity of the ionized gas ($-46 \pm 2.1 \text{ km s}^{-1}$).

information to determine absolute distances to clouds or giant molecular clouds. However, in this direction, Galactic rotation causes radial velocity to become more negative with increasing distance. On the face of it, that would place the molecular cloud on the far side of the star and nebula. However, this is possibly too naive an interpretation because, if the cloud is only tens of pc in radial extent (like its dimension in the plane of the sky), then the average shear would be too small to explain the large range in velocity (unless there were a large enhancement from a density wave).

To address the question of relative position, we made use of both the H I and CO data cubes to make an estimate of A_V produced by gas with velocities out to -45 km s^{-1} . As in § 7.2 we used the conversion factor $X = (1.9 \pm 0.5) \times 10^{20} \text{ cm}^{-2} (\text{K km s}^{-1})^{-1}$ to convert $I(\text{CO})$ to $N(\text{H}_2)$. We integrated both data cubes to obtain the atomic column densities. At the position of VES 735 we found $N(\text{H I}) = 4.5 \times 10^{21} \text{ cm}^{-2}$, assuming the emission is optically thin, and $N(\text{H}_2) = 3.1 \times 10^{21} \text{ cm}^{-2}$, the latter mostly from local rather than Perseus arm gas. Summing the contributions of atomic and molecular hydrogen we obtain the total hydrogen column density, $N_{\text{H}} = 2N(\text{H}_2) + N(\text{H I}) = 1.1 \times 10^{22} \text{ cm}^{-2}$. The total visual extinction is computed using the standard conversion factor, $A_V = 5.3 \times 10^{-22} \text{ mag cm}^{-2}$ (Bohlin, Savage, & Drake 1978). At the position of VES 735 we obtain $A_V = 5.7 \pm 0.9$, where most of the uncertainty comes from the uncertainty in the X factor (using the X factors of Digel et al. 1996 gives a lower A_V). This value of A_V compares favorably with the values around 5.7 derived by Kerton et al. (1999) using a number of methods (e.g., $B - V$ color, H α emission measure, diffuse interstellar bands). However, if the cloud's molecular column density (summed over -45 to -53 km s^{-1}) of $N(\text{H}_2) = 2.2 \times 10^{21} \text{ cm}^{-2}$ (§ 7.2) is included in the extinc-

tion calculation, then A_V rises to 8.0, which is quite inconsistent with the observed A_V to VES 735. We also made maps of the predicted extinction over the surface of the nebula for comparison with the extinction map derived by comparing H α surface brightness with radio emission (Kerton et al. 1999). Again, inclusion of the extinction from gas in the molecular cloud produces more than 2 mag too much extinction. This is strong evidence that both VES 735 and the ionized gas of KR 140 lie on the near side of the molecular cloud gas that has velocities of -45 to -53 km s^{-1} .

The extinction measurements combined with Figure 11 suggest that KR 140 could be a blister H II region on the near side of the molecular cloud. This simple geometrical interpretation of KR 140 runs into difficulty if a systematic champagne flow has developed with gas flowing away from the parent cloud at up to the sound speed of $\sim 10 \text{ km s}^{-1}$. At face value, our H α velocity implies that the ionized gas is redshifted with respect to the molecular gas, which means the H II region should be on the far side of the molecular cloud. However, it can be noted that H α is considered to be a poor line for estimating the velocity field of champagne flows (Israel 1978; Yorke, Tenorio-Tagle, & Bodenheimer 1984). Modeling of line profiles in champagne flows also shows that the velocity field can be quite random and of low amplitude, depending on geometry (Yorke et al. 1984). Recall that the geometry here is certainly not plane-parallel and probably more like a broken shell. Furthermore, our measurement sampled only gas within a projected distance of $30''$ of VES 735. Fabry-Perot data of the whole nebula in a line other than a hydrogen line would be a good way to obtain a better picture of the velocity structure of the ionized gas in KR 140.

The question then arises as to the origin of the radial velocity spread within the molecular cloud. If this is a single, gravitationally bound cloud, then this is just the virial

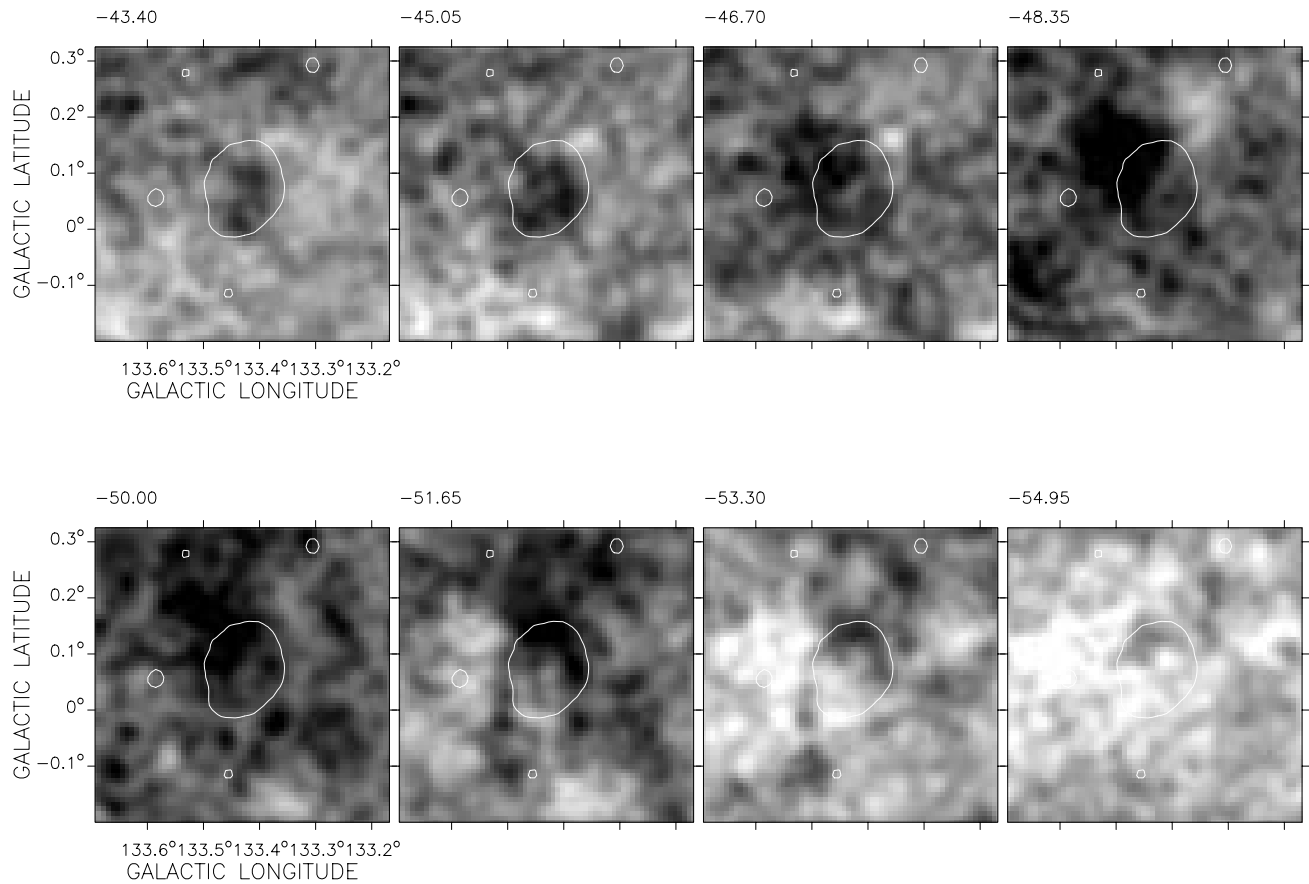


FIG. 12.—H I channel maps of the region around KR 140 from -43.40 km s^{-1} to -54.95 km s^{-1} . The H I maps have been median subtracted and are linearly scaled from -2 to 49 K (black to white). The maps have also been smoothed to $2'$ resolution for clarity. To show the extent of the ionized region, we have overlaid the 5 K contour from the 1420 MHz data.

velocity, and its mass can be estimated from

$$M_{\text{vir}} = \frac{5R\sigma^2}{\alpha_{\text{vir}} G}, \quad (11)$$

where R is the length scale for the cloud, σ is the line width, and α_{vir} is the virial parameter and includes the effects due

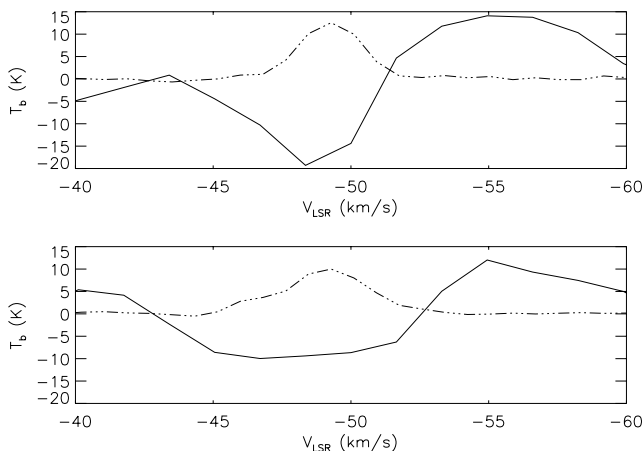


FIG. 13.—Spatially averaged CO (dashed line) and H I (solid line) spectra for (top) a region containing the CO emission to the northeast of KR 140 and (bottom) an area containing the entire H II region. The CO spectra have been multiplied by a factor of 2. The H I spectra have been median subtracted.

to surface pressure, magnetic fields, and nonuniform densities (Bertoldi & McKee 1992). As in § 7.2, we take $R = 7$ pc, and measure a typical line width to be 5 km s^{-1} (see Fig. 11). We take α_{vir} to be 1.1 (Williams & McKee 1997). With these values $M_{\text{vir}} = 1.9 \times 10^5 M_{\odot}$, which is well over an order of magnitude larger than our measured CO mass of $4.4 \times 10^3 M_{\odot}$.

This result implies that the velocity field has another origin and can significantly alter the cloud structure over time. In fact, recalling that a velocity of 1 km s^{-1} corresponds to 1 pc in 10^6 yr, one sees that the “crossing time,” $2R/\sigma$, is only 3 Myr, comparable to our above estimates of the age of VES 735 and the H II region. From the radial arrangement derived from extinction, it seems that the background molecular material is moving toward KR 140. Perhaps the parent cloud giving rise to VES 735 was the result of a converging flow or “cloud collision” that is still ongoing (relative motion in the plane of the sky would be expected too).

8. H I SIGNATURE

In theory the presence of H II regions and their surrounding molecular material should be easily visible in H I data sets: in both the ionized and molecular regions there should be a deficit of H I emission because of a lack of neutral atomic hydrogen. In addition, if the geometry is favorable, neutral atomic hydrogen associated with the PDR at the ionized-molecular interface should be visible. In practice it

is actually very difficult to observe H I features that are unambiguously associated with an H II region in raw H I data sets. This is primarily due to velocity confusion along the line of sight caused by the “turbulent” motion of the atomic gas. Since the velocity of the neutral atomic gas can be many times the typical channel width in the H I data sets velocity becomes a much poorer proxy for physical distance than in a CO data set, which is probing a species with lower velocity dispersion (heavier, cooler, and less turbulent). The situation is especially problematic for H II regions in the Galactic plane, where one has to look through a large column of atomic gas toward the H II region. For KR 140 we are looking through the local arm and part way into the Perseus arm of the Galaxy. A preliminary reconnaissance of the H I cube confirmed that the complex H I emission structure along the line of sight makes seeing any H I signal associated directly with KR 140 extremely difficult. Nevertheless, some simple processing of the H I data cube does bring out some features associated with the region.

In order to exclude local H I emission (which is assumed to have a relatively smooth spatial structure) and to enhance the dynamic range of the resulting channel maps, we constructed a median-subtracted data cube (Joncas, Durand, & Roger 1992; Joncas et al. 1985). In this technique a median spectrum is calculated for the data cube and then subtracted from each spectrum making up the cube. The resulting channel maps thus can contain both negative and positive values indicating deviations relative to the median base level.

Figure 12 shows channel maps of the median-subtracted cube over the velocity range -43.40 to -54.95 km^{-1} bracketing the ionized gas velocity of -46 ± 2.0 km s^{-1} (Kerton et al. 1999). We could not detect any features definitely associated with KR 140 in the channel maps outside of this velocity range.

Examining these maps we note the following three features. First, there is a noticeable deficit of H I seen in velocity channels -46.70 to -51.65 km s^{-1} outside of the H II region. There is excellent positional agreement between this deficit in H I and the observed position of the CO emission. The deficit can be simply interpreted as being caused by a lack of H I emission in the molecular material surrounding KR 140. Second, we also see a drop in the H I emission occurring within the H II region in the -43.40 and -45.05 km s^{-1} channels. This deficit is most likely associated with the ionized gas in KR 140 as suggested by their spatial correspondence. Figure 13 presents spatially averaged H I and CO spectra for an area just outside of the H II region to the northeast and the area inside the H II region. The anticorrelation between H I emission and the presence of CO and H II is evident. Third, there is an enhancement of H I emission at $(133^{\circ}36, 0^{\circ}1583)$, seen best in the velocity channel -46.70 km s^{-1} . This could be low velocity dispersion material associated with the PDR. Atomic material in the PDR is expected to have low velocity and thus should be seen in channels corresponding to CO emission.

9. THE ENVIRONMENT OF KR 140

9.1. Spontaneous Massive Star Formation

In the context of the Perseus Arm star formation activity, the KR 140 complex seems to be unique. Figure 1 shows that KR 140 is isolated from the massive and violent star formation that is ongoing around it. This isolation is evi-

dence to us that KR 140 is an example of massive star formation in our Galaxy that is *untriggered*, at least in the sense used in the context of sequential star formation. In none of our data sets does there appear any evidence for a trigger of the star formation in KR 140. The exciting cluster of W4, OCl 352, is about 60 pc away from KR 140, for a cluster distance of 2.35 kpc (Massey, Johnson, & DeGioia-Eastwood 1995). For a sound speed of 0.6 km s^{-1} (isothermal speed in H_2 at 100 K), the time for a signal to reach KR 140 would be about 90 Myr, much greater than our estimated age of KR 140 of a few million years or the age of OCl 352. From W3, a signal would take about 60 Myr, but W3 is itself much less than 10^5 yr old (Kawamura & Masson 1998). The supernova remnant HB 3 is also in this complex (Normandeau et al. 1997), but, from Figure 1, the edge of the remnant is nowhere near to KR 140. Thus, KR 140 does not seem to be triggered by a neighboring H II region or a nearby supernova remnant, unless the impulse came along the line of sight. This conclusion is complemented by the overall smoothness of the KR 140 nebula; while the nebula does show density inhomogeneities, it is not far removed from a circular shape. Thus, any perturbation that might have triggered the star formation within KR 140 must have been a large scale phenomenon with a characteristic scale of ~ 10 pc. This kind of triggering might be more consistent with triggering via a spiral density wave (e.g., Elmegreen 1994, 1995) or by colliding molecular clouds. Of course, we cannot rule out those kinds of triggers, but the observational evidence would be difficult to find.

It is interesting to contrast KR 140 to another star-forming region that has been studied with multiwavelength data, the Gemini OB 1 molecular complex (Carpenter, Snell, & Schloerb 1995a, 1995b). Within the molecular complex, these authors find young star clusters (from near-infrared data) and a number of dense cores (as identified by CS observations) associated with *IRAS* point sources. Carpenter et al. suggest that the arc-shaped morphologies of these cores have been formed by swept-up gas from expanding H II regions and that they would form the massive star clusters in the region. The other lower infrared luminosity sources (most likely belonging to lower mass cores) in the Gem OB 1 complex are not found to be correlated with any arc-shaped structures or filaments in the molecular gas, and they are not adjacent to any H II regions; in fact, they are spread almost randomly around the complex. Carpenter et al. therefore conclude that induced star formation is the prominent mode of formation for massive stars in the Gem OB 1 molecular complex.

If KR 140 is indeed untriggered, then it seems to be an unusual form of spontaneous star formation, since current observations suggest that the isolated mode of star formation is generally associated with low-mass star-forming regions as seen in Gem OB 1 or even in Taurus.

9.2. *IRAS* Point Sources and Protostars

As has been seen in other sites in the Galaxy, an H II region can initiate star formation via the expansion of its ionization front (e.g., Elmegreen & Lada 1977). Other stars might also have formed spontaneously. Evidence for other star-forming regions within KR 140 may be sought by examining the *IRAS* point source catalog. In addition to the *IRAS* point source 02165 + 6053 that is cross-referenced to VES 735, there are six other *IRAS* point sources in the

TABLE 3
IRAS POINT SOURCES NEAR KR 140

<i>IRAS</i>	<i>l</i> (deg)	<i>b</i> (deg)	Notes
02168 + 6052.....	133.49	0.07	Part of dust shell
02160 + 6057.....	133.37	0.12	Part of dust shell
02157 + 6053.....	133.35	0.04	Part of dust shell; molecular core
02171 + 6058.....	133.49	0.17	No CS or CH ₃ OH detection; colors of UCH II region
02174 + 6052.....	133.56	0.09	Not associated (?)
02156 + 6045.....	133.39	-0.08	Not associated (?)

area in and around KR 140 (see Table 3). The crosses in Figure 14 show the positions of these six *IRAS* point sources. The circled crosses are the sources discussed here that seem most likely to be associated with the KR 140 complex.

The source *IRAS* 02160 + 6057 identified with the northwest dust arc has been the subject of two molecular line investigations. Wouterloot & Brand (1989) identified it as a potential star-forming area via its *IRAS* colors (see their paper for the exact selection criteria), and examined it (along with about 1300 other *IRAS* point sources) for CO emission. They found a CO feature in that direction at a velocity of -49.7 km s^{-1} (LSR), which corresponds to CO in the associated background molecular cloud, and assigned it the catalog number [WB89] 417. This point source was then observed in an H₂O line by Wouterloot, Brand, & Fiegle (1993), but they were unable to detect any emission. This line of sight has one of the highest column densities in the KR 140 H II region, so it is possible that a protostar could be forming there as a result of the expansion of the H II region. However, examination of the HIRES images shows no pointlike features in the dust arc, and none are found in follow-up submillimeter observations with

SCUBA (C. R. Kerton et al. 2000, in preparation). Therefore, *IRAS* 02160 + 6057 is most likely simply part of the KR 140 dust shell. Likewise, *IRAS* 02168 + 6052 appears to just be part of the eastern side of the dust shell; it has not been the subject of any molecular line observations.

The source *IRAS* 02157 + 6053 also seems to have been an identification of some part of the dust shell. In the submillimeter there is more structure in this region; this object appears to be a molecular core rather than a protostar (Kerton et al. 2000, in preparation).

The point source *IRAS* 02171 + 6058 is identified with the dust feature to the north of the KR 140 complex. It was included in a CS(2-1) survey by Bronfman, Nyman, & May (1996) of *IRAS* point sources that have colors characteristic of ultracompact H II regions; however, they were unable to make a detection. Lyder & Galt (1997) observed this source along with other ultracompact H II region candidates in a search for methanol maser emission. Again, they were unable to detect any maser emission from *IRAS* 02171 + 6058. These nondetections do not rule out the possibility that the source is a protostar. In fact there is a submillimeter detection, and all evidence seems consistent with a B5 V star (Kerton et al. 2000, in preparation). It is outside the radio contours of H II region and is therefore difficult to interpret as being triggered.

A photographic survey of the W3 and W4 region turned up bright infrared stars (BIRS; Elmegreen 1980) that are brighter in the *I* band than in the *R* band. There are five of these stars in the KR 140 region of the sky. Table 4 gives their coordinates along with their *R* and *I* magnitudes, and the positions are indicated by triangles on Figure 14. Elmegreen (1980) estimated that if these stars were at the distance of the Perseus arm then they might be deeply embedded massive early or pre-main-sequence stars, or even giants or supergiants. From examining the overall distribution of the BIRS stars (Fig. 1 in Elmegreen 1980), we find there is an overabundance of BIRS around KR 140 as compared to the average. It is difficult to say whether or not these BIRS stars are physically associated with the KR 140 complex. However, BIRS 128 on the eastern side of the

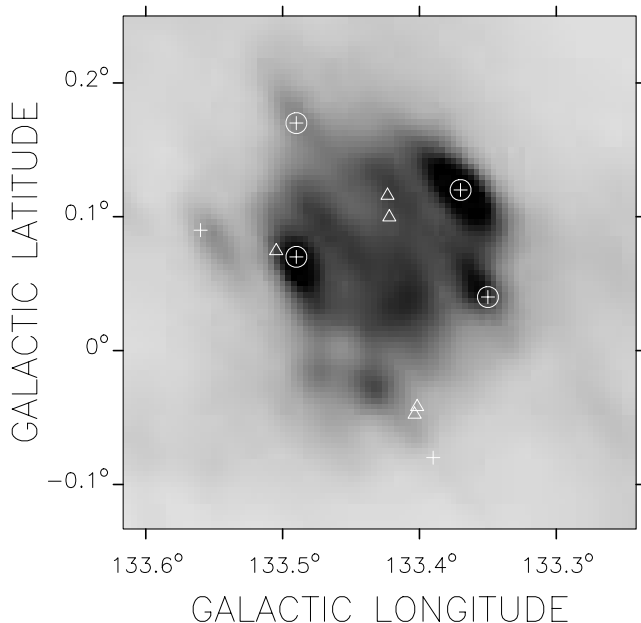


FIG. 14.—*IRAS* point sources (crosses) and BIRS positions (triangles) near KR 140. Circled crosses indicate point sources probably associated with KR 140. The linear gray scale for the $60 \mu\text{m}$ image is $0\text{--}185 \text{ MJy sr}^{-1}$ (white to black).

TABLE 4
 BRIGHT INFRARED STARS (BIRS) NEAR KR 140

Star	<i>l</i> (deg)	<i>b</i> (deg)	<i>R</i>	<i>I</i>
BIRS 128.....	133.50472	0.07443	20.5	13.8
BIRS 129.....	133.42336	0.11588	19.6	13.1
BIRS 130.....	133.42205	0.09973	20.5	13.8
BIRS 131.....	133.40169	-0.04194	18.7	13.6
BIRS 132.....	133.40358	-0.04767	18.0	13.7

nebula seems to lie at a well-defined edge of the dust shell and within the CO shell.

9.3. The Gas Cloud

We have been able to estimate some properties of the original molecular cloud that spawned the KR 140 H II region. Originally having $M \sim 4.9 \times 10^3 M_\odot$, this cloud would then be classified as a dwarf molecular cloud. These are quite numerous in the ISM. The column density of $2.2 \times 10^{21} \text{ cm}^{-2}$ is about the same as the median column density of $2 \times 10^{21} \text{ cm}^{-2}$ in the molecular gas in the outer Galaxy (Heyer et al. 1998). Once VES 735 formed in the molecular cloud, it had a tremendous impact on the environment around it. It has incorporated $25 M_\odot$, ionized about $160 M_\odot$, and a further $290 M_\odot$ of cloud material has been removed since the ionization front broke out of the front part of the molecular cloud. The remnant cloud is of fairly low density, $n_{\text{H}_2} \sim 100 \text{ cm}^{-3}$.

The velocity width of the molecular cloud is too large for the cloud to be bound, but it is unlikely to arise from velocity shear due to differential Galactic rotation. It is possible to interpret the velocity structure as a large scale flow of material toward KR 140. If true, this flow could have had an impact on the star formation history of this region.

We can use our estimate of the original molecular cloud mass to estimate the mass of the stellar cluster that likely formed along with VES 735. Hunter et al. (1990) observed clouds in our mass range and estimated cluster masses using a Miller-Scalo initial mass function (IMF; Miller & Scalo 1979). Using their data we find the correlation shown in Figure 15: $\log M_{\text{cluster}} = (0.254 \pm 0.111) \log M_{\text{cloud}} + (2.306 \pm 0.449)$. With the above cloud mass we estimate a cluster mass of about $1.7 \times 10^3 M_\odot$. Of course, since we know the mass of the most massive star we can use a Miller-Scalo IMF to estimate the mass of the cluster directly. Using

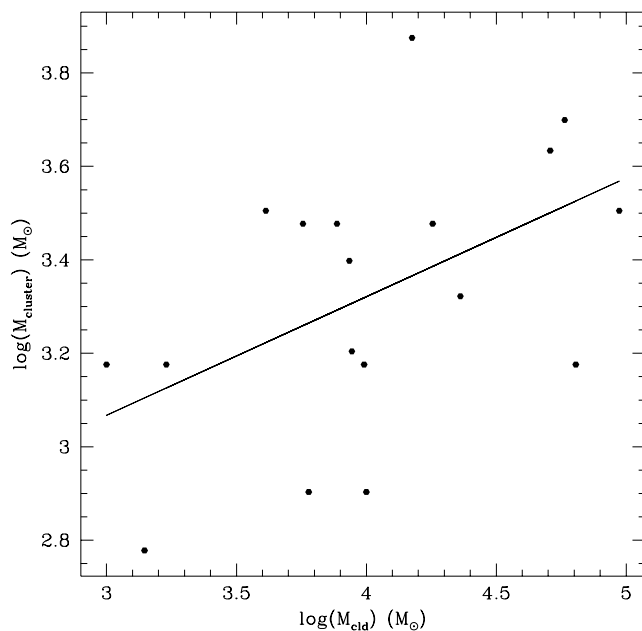


FIG. 15.—Correlation between the mass of a molecular cloud and the mass of the stellar cluster that has formed within the cloud. Derived from data given by et al. (1990). The rms scatter in the relation is 0.245 dex.

equation (12) in Elmegreen (1983) we estimate a cluster mass of about $1.6 \times 10^3 M_\odot$, consistent with the above “empirical” estimate. Using these cluster and cloud masses, we estimate a star formation efficiency [SFE = $M_{\text{cluster}} / (M_{\text{cluster}} + M_{\text{cloud}})$] of about 25%, which is typical for clouds of this size (Hunter et al. 1990), although values can range over 2 orders of magnitude from cloud to cloud (Williams & McKee 1997). This low value of the SFE implies that the cluster within KR 140 will not be gravitationally bound.

Near-infrared observations (such as ones in the ongoing 2MASS survey) should be able to detect a number of pre-main-sequence stars from this cluster around VES 735. It would be interesting to compare the IMF in this region to the IMF in regions where the star formation was triggered. Which, if either, is a good description of the IMF in the Galaxy?

10. CONCLUSIONS

We have utilized our multiwavelength data set (all at a resolution of about $1'$) to study not only the physics of the H II region itself, but also, since the data are from the larger CGPS survey, to study KR 140 in the context of the overall picture of star formation in the Perseus spiral arm. We find no evidence for a mechanism that triggered the formation of the O8.5 V(e) star, VES 735, and its (largely unseen) cluster. We therefore conclude that this region formed spontaneously out of its parent molecular cloud, independent of the more vigorous star formation in W3 and W4 nearby.

Our data of KR 140 are consistent with the model of a bowl-shaped region viewed close to face-on. Extinction measurements to the exciting star, VES 735, and nebula show that the H II region is quite likely on the near side of its molecular cloud. We have not observed any champagne flow and cannot rule out other geometries. KR 140 has an age less than a few million years. We have estimated that the original molecular cloud had a mass of $4.9 \times 10^3 M_\odot$ and an average density about 100 cm^{-3} , which classifies it as a dwarf molecular cloud. This makes KR 140 even more unusual as it is a rare example of an O star that has formed in a cloud with a mass less than $10^4 M_\odot$. There is tentative evidence that the molecular material is undergoing a large-scale flow toward KR 140. Follow-up observations are needed to pursue this idea. There are four IRAS point sources associated with the KR 140 complex, one of which is a possible protostar candidate and another a molecular core. Near-infrared observations of KR 140 are needed to find and study the young cluster that likely formed along with VES 735.

We would like to thank Gary Ferland for his assistance with the use of Cloudy and Doug Johnstone for helpful discussions. We also acknowledge useful comments by the referee, Peter Barnes. This research made use of the SIMBAD data base, operated at CDS, Strasbourg, France. This research was supported by the Natural Sciences and Engineering Research Council of Canada. D. R. B. participated originally via the Physics Co-op program of the University of Victoria.

REFERENCES

- Allamandola, L. J., Tielens, A. G. G. M., & Barker, J. R. 1985, *ApJ*, 290, L25
- Becker, R. H., White, R. L., & Edwards, A. L. 1991, *ApJS*, 75, 1
- Bertoldi, F., & McKee, C. F. 1992, *ApJ*, 395, 140
- Bidelman, W. P. 1988, *Bull. Inf. CDS*, 35, 52
- Blitz, L. 1993, in *Protostars and Planets III*, ed. E. H. Levy & J. I. Lunine (Tucson: Univ. Arizona Press), 125
- Bohlin, R. C., Savage, B. D., & Drake, J. F. 1978, *ApJ*, 224, 132
- Boulanger, F., Baud, D., & van Albada, G. D. 1985, *A&A*, 114, L9
- Boulanger, F., Beichman, C., Désert, F. X., Helou, G., Pérault, M., & Ryter, C. 1988, *ApJ*, 332, 328
- Braunsfurth, E. 1983, *A&A*, 117, 297
- Bregman, J. D., Sloan, G. C., Schultz, A. S. B., Temi, P., & Rank, D. M. 1995, *BAAS*, 27, 1314
- Bronfman, L., Nyman, L.-Å., & May, J. 1996, *A&AS*, 115, 81
- Cao, Y., Terebey, S., Prince, T. A., & Beichman, C. A. 1997, *ApJS*, 111, 387
- Carpenter, J. M., Snell, R. L., & Schloerb, F. P. 1995a, *ApJ*, 445, 246
- . 1995b, *ApJ*, 450, 201
- Castor, J., McCray, R., & Weaver, R. 1975, *ApJ*, 200, L107
- Chieffi, A., Limongi, M., & Straniero, O. 1998, *ApJ*, 502, 737
- Clarke, C. J., Bonnell, I. A., & Hillenbrand, L. A. 2000, in *Protostars and Planets IV*, ed. V. Mannings, A. P. Boss, & S. S. Russell (Tucson: Univ. Arizona Press), in press
- Comerón, F. 1997, *A&A*, 326, 1195
- Cox, P. 1990, *A&A*, 236, L29
- Dickel, H. 1980, *ApJ*, 238, 829
- Digel, S. W., Lyder, D. A., Philbrick, A. J., Puche, D., & Thaddeus, P. 1996, *ApJ*, 458, 561
- Dorland, H., Montmerle, T., & Doom, C. 1986, *A&A*, 160, 1
- Elmegreen, B. G. 1983, *MNRAS*, 203, 1011
- . 1985, in *Protostars and Planets II*, ed. D. C. Black & M. S. Matthews (Tucson: Univ. Arizona Press), 33
- . 1992, in *Star Formation in Stellar Systems*, ed. G. Tenorio-Tagle, M. Prieto, & F. Sanchez (Cambridge: Cambridge Univ. Press), 381
- . 1994, *ApJ*, 433, 39
- . 1995, in *The Formation of the Milky Way*, ed. E. J. Alfaro & A. J. Delgado (Cambridge: Cambridge Univ. Press), 28
- Elmegreen, B. G., Efremov, Y., Pudritz, R. E., & Zinnecker, H. 2000, in *Protostars and Planets IV*, ed. V. Mannings, A. P. Boss, & S. S. Russell (Tucson: Univ. Arizona Press), in press
- Elmegreen, B. G., & Lada, C. J. 1977, *ApJ*, 214, 725
- Elmegreen, D. M. 1980, *ApJ*, 240, 846
- Emerson, J. P. 1988, in *Formation and Evolution of Low-Mass Stars*, ed. A. K. Dupree & M. T. V. T. Lago (Dordrecht: Kluwer), 193
- English, J., et al. 1998, *Publ. Astron. Soc. Australia*, 15, 56
- Ferland, G. J. 1996, *Hazy: A Brief Introduction to Cloudy*, Internal Rep., Univ. Kentucky Dept. Phys. Astron
- Ferland, G. J., Korista, K. T., Verner, D. A., Ferguson, J. W., Kingdon, J. B., & Verner, E. W. 1998, *PASP*, 110, 761
- Franco, J., Shore, S. N., & Tenorio-Tagle, G. 1994, *ApJ*, 436, 795
- Giard, M., Bernard, J. P., Lacombe, F., Normand, P., & Rouan, D. 1994, *A&A*, 291, 239
- Gordon, M. A. 1988, in *Galactic and Extragalactic Radio Astronomy*, ed. G. L. Verschuur & K. I. Kellermann (New York: Springer), 37
- Gregory, P. C., & Taylor, A. R. 1986, *AJ*, 92, 371
- Heyer, M. H., Brunt, C., Snell, R. L., Howe, J. E., Schloerb, F. P., & Carpenter, J. M. 1998, *ApJS*, 115, 241
- Heyer, M. H., & Terebey, S. 1998, *ApJ*, 502, 265
- Heyer, M. H., et al. 1996, *ApJ*, 464, L175
- Hjellming, R. M. 1968, *ApJ*, 154, 533
- Hunter, D. A., Thronson, H. A., Jr., & Wilton, C. 1990, *AJ*, 100, 1915
- Israel, F. P. 1978, *A&A*, 70, 769
- Joint *IRAS* Science Working Group. 1988, *IRAS Point Source Catalog, Version 2* (Washington: GPO)
- Joncas, G., Dewdney, P. E., Higgs, L. A., & Roy, J. R. 1985, *ApJ*, 298, 596
- Joncas, G., Durand, D., & Roger, R. S. 1992, *ApJ*, 387, 591
- Kallas, E., & Reich, W. 1980, *A&AS*, 42, 227
- Kawamura, J. H., & Masson, C. R. 1998, *ApJ*, 509, 270
- Kerton, C. R. 1999, Ph.D. thesis, Univ. Toronto
- Kerton, C. R., Ballantyne, D. R., & Martin, P. G. 1999, *AJ*, 117, 2485
- Kerton, C. R., & Martin, P. G. 2000, *ApJS*, 126, 85
- Kim, S.-H., Martin, P. G., & Hendry, P. D. 1994, *ApJ*, 422, 164
- Lada, C. J., Elmegreen, B. G., Cong, H.-I., & Thaddeus, P. 1978, *ApJ*, 226, L39
- Lagache, G., Abergel, A., Boulanger, F., & Puget, J.-L. 1998, *A&A*, 333, 709
- Laor, A., & Draine, B. T. 1993, *ApJ*, 402, L441
- Léger, A., & Puget, J. L. 1984, *A&A*, 137, L5
- Loren, R. B. 1976, *ApJ*, 209, 466
- . 1977, *ApJ*, 218, 716
- Lyder, D. A., & Galt, J. 1997, *AJ*, 113, 1310
- Massey, P., Johnson, K. E., & DeGioia-Eastwood, K. 1995, *ApJ*, 454, 151
- Miller, G., & Scalo, J. 1979, *ApJS*, 41, 513
- Normandeau, M., Taylor, A. R., & Dewdney, P. E. 1997, *ApJS*, 108, 279
- Onaka, T., Yamamura, I., Tanabé, T., Roellig, T. L., & Yeun, L. 1996, *PASJ*, 48, L59
- Oster, L. 1961, *Rev. Mod. Phys.*, 33, 525
- Osterbrock, D. E. 1989, *Astrophysics of Gaseous Nebula and Active Galactic Nuclei* (Mill Valley, CA: University Science)
- Panagia, N. 1973, *AJ*, 78, 929
- Patel, N. A., Goldsmith, P. F., Heyer, M. H., Snell, R. L., & Pratap, P. 1998, *ApJ*, 507, 241
- Roger, R. S., Costrain, C. H., Lacey, J. D., Landecker, T. L., & Bowers, F. K. 1973, *Proc. IEEE*, 61, 1270
- Roger, R. S., & Irwin, J. A. 1982, *ApJ*, 256, 127
- Schaerer, D., & de Koter, A. 1997, *A&A*, 322, 598
- Scofield, N. Z., Sanders, D. B., & Clemens, D. P. 1986, *ApJ*, 310, L77
- Sellgren, K. 1984, *ApJ*, 277, 623
- Shu, F. H., Adams, F. C., & Lizano, S. 1987, *ARA&A*, 25, 23
- Spitzer, L., Jr. 1978, *Physical Processes in the Interstellar Medium* (New York: Wiley)
- Storey, P. J., & Hummer, D. G. 1995, *MNRAS*, 272, 41
- Strömgren, B. 1939, *ApJ*, 89, 529
- Strong, A. W., & Mattox, J. R. 1996, *A&A*, 308, L21
- Taylor, A. R. 1999, in *ASP Conf. Ser. 168, New Perspectives on the Interstellar Medium*, ed. A. R. Taylor, T. L. Landecker, & G. Joncas (San Francisco: ASP), 3
- Taylor, A. R., & Gregory, P. C. 1983, *AJ*, 88, 1784
- Tenorio-Tagle, G. 1979, *A&A*, 71, 59
- Thronson, H. A., Lada, C. J., & Hewagama, T. 1985, *ApJ*, 297, 662
- Usami, M., Hanawa, T., & Fujimoto, M. 1995, *PASJ*, 47, 271
- Vallée, J. P., Hughes, V. A., & Viner, M. R. 1979, *A&A*, 80, 186
- van der Werf, P. P., & Goss, W. M. 1990, *A&A*, 238, 296
- Veidt, B. G., Landecker, T. L., Vaneldik, J. F., Dewdney, P. E., & Routledge, D. 1985, *Radio Sci.*, 20, 1118
- Wen, Z., & O'Dell, C. R. 1995, *ApJ*, 438, 784
- Westerhout, G. H. 1958, *Bull. Astron. Instit. Netherlands*, 14, 215
- Whitworth, A. 1979, *MNRAS*, 186, 59
- Wilking, B. A., Harvey, P. M., Lada, C. J., Joy, M., & Doering, C. R. 1984, *ApJ*, 279, 291
- Williams, J. P., & McKee, C. F. 1997, *ApJ*, 476, 166
- Wouterloot, J. G. A., & Brand, J. 1989, *A&AS*, 80, 149
- Wouterloot, J. G. A., Brand, J., & Fiegle, K. 1993, *A&AS*, 98, 589
- Yorke, H. W. 1986, *ARA&A*, 24, 49
- Yorke, H. W., Tenorio-Tagle, G., & Bodenheimer, P. 1983, *A&A*, 127, 313
- . 1984, *A&A*, 138, 325
- Yorke, H. W., Tenorio-Tagle, G., Bodenheimer, P., & Różyczka, M. 1989, *A&A*, 216, 207
- Zhang, X., & Higgs, L. 1997, *Chinese A&A*, 21, 129